SHEAR STRENGTH AND YIELD SURFACE OF A PARTIALLY SATURATED SANDY SILT UNDER GENERALIZED STRESS STATES

Rodrigo C. Weber, Ph. D[1], Enrique Romero, Ph. D.[2] and Antonio Lloret, Ph. D.[3]

Affiliation:

[1] Universitat Politècnica de Catalunya, Department of Civil and Environmental Engineering, c/Jordi Girona 1-3, 08034 Barcelona, Spain; e-mail: rodrigow7@yahoo.com.br

[2] Universitat Politècnica de Catalunya, Department of Civil and Environmental Engineering, c/Jordi Girona 1-3, 08034 Barcelona, Spain; e-mail: enrique.romero-morales@upc.edu

International Centre for Numerical Methods in Engineering, c/Gran Capità s/n, 08034 Barcelona, Spain.

[3] Universitat Politècnica de Catalunya, Department of Civil and Environmental Engineering, c/Jordi Girona 1-3, 08034 Barcelona, Spain; e-mail: antonio.lloret@upc.edu

***Corresponding author:** Rodrigo C. Weber

Telephone: +5551999020966
Fax:
E-mail: rodrigow7@yahoo.com.br

Abstract

This paper studies the hydromechanical behavior of a slightly compacted mixture of sand and clayey silt (30%/70%) under a generalized stress state. The experimental study focused on analyzing the yielding response and shear strength behavior at different stress states (characterized by the intermediate principal stress parameter *b*, or Lode angle) and at different initial total suctions (as-compacted state). For the investigation, a hollow cylinder apparatus was used. The shear strength results allowed defining the variation of the critical state line with the Lode angle and the suction. Different models were proposed for isotropic and anisotropic yield surfaces, and their shape and rotation were calibrated with experimental results. The modeled yield surfaces fitted reasonably well the experimental results, considering their inclination and dependence on the suction, mean and deviatoric stresses and Lode angle. In addition, some relationships between the stresses and the model parameters were proposed to normalize the yield surface equation.

Keywords: unsaturated soils; generalized stress state; shear strength; yield surface; Lode angle

NOTATION

b parameter for intermediate principal stress $(\sigma_2-\sigma_3)/(\sigma_1-\sigma_3)$

c cohesion $\frac{s}{m+n\,s}$

d dilatancy $\frac{\Delta\varepsilon_v^p}{\Delta\varepsilon_q^p}$

e void ratio

f, g yield and plastic potential functions

f_1, g_1 fitting parameters in p_m versus ln $(1+s)$ relationship

G elastic shear modulus

L stress vector modulus $\sqrt{\Delta\sigma_1^2+\Delta\sigma_2^2+\Delta\sigma_3^2}$

M critical state line slope

m and n parameters for the variation of cohesion with suction

p net mean stress $(\sigma_1+\sigma_2+\sigma_3)/3$

p_0 isotropic initial preconsolidation stress

p_f, q_f net mean and deviatoric stresses at failure

p_m parameter that defines the size of the inclined yield surface (Romero and Jommi, 2008)

$p_s = c(s)/\tan\phi$ contribution of suction to correct mean stress:

$\hat{p} = p + p_s$

q deviatoric stress $\frac{1}{\sqrt{2}}\sqrt{(\sigma_1-\sigma_2)^2+(\sigma_2-\sigma_3)^2+(\sigma_1-\sigma_3)^2}$

r,t fitting parameters in M_α versus b relationship

s suction (total)

Sr degree of saturation

W axial load

w water content

W_p accumulated plastic work per unit soil volume

α_σ inclination of major principal stress relative to the vertical direction $\frac{1}{2}\tan^{-1}(2\tau_{\theta z}/(\sigma_1-\sigma_3))$

α, μ parameters in Lagioia's model (Lagioia et al., 1996)

ε_z, ε_r, ε_θ vertical, radial and circumferential strains

ε_1, ε_2, ε_3 principal strains

ε_v, ε_v^e, ε_v^p volumetric strains: total, elastic and plastic

ε_q shear strain $\frac{\sqrt{2}}{3}\sqrt{(\varepsilon_1-\varepsilon_2)^2+(\varepsilon_2-\varepsilon_3)^2+(\varepsilon_1-\varepsilon_3)^2}$

ϕ friction angle

η stress ratio or obliquity $q/(p+p_s)$

σ'_{v0} saturated preconsolidation vertical stress

σ_z, σ_r, σ_θ vertical, radial and circumferential stresses

σ_1, σ_2, σ_3 principal stresses

θ rotation angle in hollow cylinder tests

θ_L Lode angle $\tan^{-1}((2b-1)/\sqrt{3})$

$\tau_{\theta z}$ shear stress in the vertical plane

1 INTRODUCTION

The stress state in many engineering applications is different from that usually considered in elastoplastic models under axisymmetric stress state conditions. Therefore, constitutive models to be used in the analyses of engineering problems such as foundations, earth dams, and embankments should take into account experimental information that comes from stress-strain tests in a generalized stress state (Nasreddine, 2004; Zerfa and Loret, 2003; Grammatikopoulou et al., 2007; Zhang et al., 2010; Zhang et al., 2016; Yao and Yang, 2017; Yan et al., 2020; Li et al., 2021).

Several authors have used true triaxial apparatus and hollow cylinder devices to perform tests to study the influence of the intermediate principal stress on mechanical soil behavior in saturated conditions (Matsuoka and Nakai,1974; Hight et al., 1983; Matsuoka et al., 1995; Yoshimine et al., 1998; Nishimura et al. 2007; Yimsiri et al., 2011; Minaeian et al., 2020), and more recently in unsaturated conditions at constant matric suction (Hoyos, 1998; Macari and Hoyos, 2001; Toyota et al., 2001; Matsuoka et al., 2002; Macari et al., 2003; Toyota et al., 2003; Toyota et al., 2004; Hoyos et al. 2012a; Hoyos et al., 2015; Jafarzadeh at al. 2019; Zheng et al., 2020 and 2021). Nevertheless, to the authors' best knowledge, the effect of intermediate stress in the shape of the yield surface in anisotropic elastoplastic models in unsaturated soils has not been studied in depth in laboratory tests under generalized stresses.

The effect of the intermediate principal stress on soil shear strength has been considered using diverse approaches. The Mohr-Coulomb envelop (Yoshimine, 2006; Maïolino and Luong, 2009), the spatially mobilized plane (SMP) criterion (Matsuoka and Nakai,1974; Matsuoka and Sun, 1995) and the Lade-Duncan criterion (Lade and Duncan, 1975; Lade, 1997) have been widely used. Wojciechowski (2018) has analyzed the differences between Mohr-Coulomb and Drucker-Prager criteria, and Wang et al. (2019) have

proposed a nonlinear unified criterion for saturated geo-materials. Concerning unsaturated materials, Sun et al. (2000) have suggested an extension of SMP for unsaturated soils, whereas Zhang et al. (2015) have proposed a linear unified failure criterion for unsaturated soils. Thus, the increase in soil strength due to suction can be considered as a linear relationship (Fredlund et al., 1978; Alonso et al. 1990) or as a nonlinear relationship (Escario and Saez, 1986; Fredlund et al., 1987; Sun et al., 2000; Vanapalli, S. K., 2009; Sheng et al., 2011).

Many elastoplastic constitutive models have been used during the last three decades, taking into account generalized stress states in partially saturated soils. Matsuoka et al. (1999); Yao et al. (2009); Ma et al. (2017); Wang et al. (2019) and Lu et al. (2019) summarize available methodologies to extend the existing constitutive models for triaxial compression conditions to be suitable for 3D stress states (i.e., indirect methods) or to adopt 3D yield and plastic potential functions based on observed soil behavior (i.e., direct methods).

Kohgo et al. (1993) proposed a constitutive model that defined the yield surface using the generalized Coulomb criterion and an elliptical cap model, both as a function of Lode's angle. Matsuoka et al. (2002), Sun et al., 2000 and Sun et al., 2003 simulated the measured stress–strain-strength behavior of unsaturated sand, tested under controlled suction in a true triaxial device using elastoplastic models based on SMP. The same procedure was used by Sun et al. (2007a; 2007b), incorporating the hysteresis of the degree of saturation in their model. In the last decade, other models have included the degree of saturation in the constitutive variables (Romero and Jommi, 2008; Lloret-Cabot et al., 2013; Li et al., 2019).

Macari et al. (2003) and Hoyos et al. (2012,b) obtained reasonably accurate results modeling true triaxial tests on unsaturated cubic specimens based on the Barcelona Basic

Model (Alonso et al., 1990) and Wheeler and Sivakumar (1995) elastoplastic models. Georgiadis et al. (2005) developed an elastoplastic model using a modified version of Lagioia et al. (1996) yield function and plastic potential. Maleki and Pouyan (2016) proposed a kinematic hardening model adapting CJS (Cambou–Jafari and Sidoroff) model to the unsaturated state. Lastly, some numerical models have been proposed for expansive soils under generalized stress states to model the behavior of backfills and seals used in deep radioactive waste disposal, some numerical models have been proposed for expansive soils under generalized stress states (Sánchez et al., 2005; Kohler and Hofstetter, 2008; Della Vecchia et al. 2012).

In addition, laboratory test campaigns on isotropically and anisotropically compacted specimens and constitutive models have been proposed to investigate the evolution of induced anisotropy in unsaturated soils. The anisotropically compacted specimens presented distorted yield ellipses in the constant suction plane with no substantial influence on the critical state line (Cui and Delage, 1996; Romero et al., 2003; Della Vecchia et al., 2012; Al-Sharrad and Gallipoli, 2016; Al-Sharrad et al., 2017; Sitarenios and Kavvadas, 2020).

Romero et al. (2017) carried out hydromechanical tests using a hollow cylinder apparatus on a partially saturated sand/silt mixture, which was prepared for high water permeability, adequate strength for handling, and collapsibility on wetting. In addition to shear strength tests at constant water content, soaking tests were done on unsaturated samples to determine the collapse potential of the soil under constant mean (p) and deviatoric (q) stresses with different values of the parameter for intermediate principal stress b.

Seeking to continue the study by Romero et al. (2017), a new contribution to the current state of the knowledge on partially saturated soils is presented based on an experimental study of the effect of suction and stress state on the hydromechanical (HM) behavior of

an anisotropically compacted fine soil. The present study focuses on the evolution of the size and the shape of the yield surface while following different generalized stress paths, as well as on the shear strength properties.

2 SOIL MIXTURE DESCRIPTION AND INITIAL STATE

A sand/silt mixture was prepared for the experimental campaign. The sand is a poorly graded fine from Castelldefels beach (Llobregat Delta, near Barcelona) with particle sizes between 150 µm and 1.18 mm and solids' density ρ_s=2.65 Mg/m^3 (Cárdenas et al., 2015). The finer fraction corresponds to clayey silt from Barcelona (LL=36%; IP=19% and ρ_s=2.67 Mg/m^3) (Barrera, 2002; Alonso et al., 2013; Romero et al., 2019). The soil mixture was used to reach high permeability (k~10^{-7} m/s) and adequate strength for handling and executing the planned tests. A first attempt was made to use the sand/silt mixture sample similar to the one used by Romero et al. (2017) to extend further their results. However, a slightly higher fine content was used to improve the strength for handling. The grain size distribution curves of the materials, including the one used by Romero et al. (2017), are shown in Figure 1.

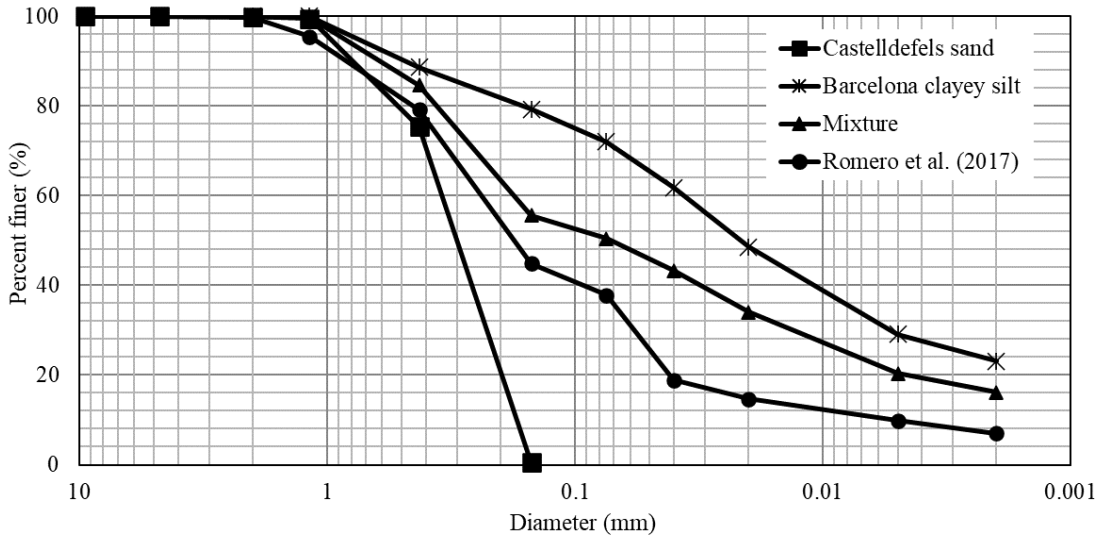

Figure 1. Grain size distribution of the materials.

It was necessary to perform preliminary tests on mixtures with different amounts of clayey silt and sand to select the adequate percentage of each type of material present in the sample. The samples' stability in handling was verified with unconfined compression tests on compacted samples with low moisture content. Samples were statically compacted under oedometer conditions until they reached a dry density of 1.65 Mg/m^3. The samples were compressed by both sides (top and bottom) to ensure the sample's homogeneity throughout the height. The results of unconfined compression tests are shown in Figure 2, which concluded that the best mixture was for 70% clayey silt and 30% sand (as shown in Figure 1).

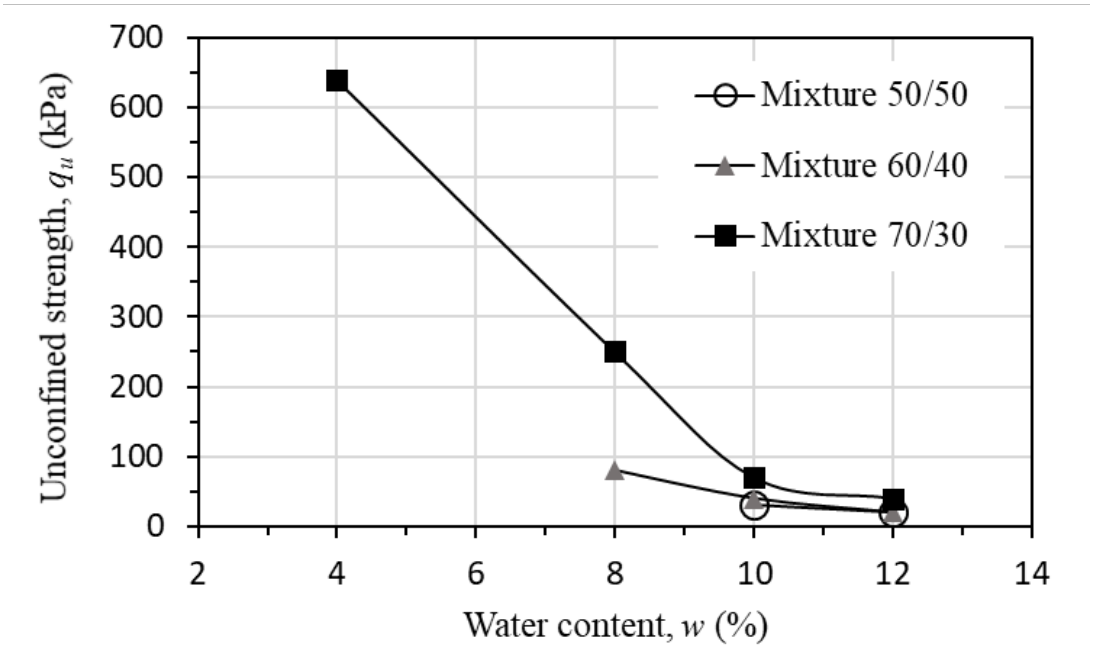

Figure 2. Unconfined compression strength for different mixture proportions (clayey silt/sand) and water content at compaction.

The water retention curves show small hysteresis in drying/wetting cycles after the first drying (Figure 3a). In addition, changes in the porosity of the samples have a small effect on the total suction at given water content (Figure 3b). Finally, the selected mixture has been prepared with a dry density of 1.65 Mg/m^3 at water contents of w=4.0%, 6.0%, and

8.0% (S_r=0.17, 0.26, and 0.32) corresponding to total suctions close to s=16.0, 1.5, and 0.2 MPa, respectively (Figure 3b).

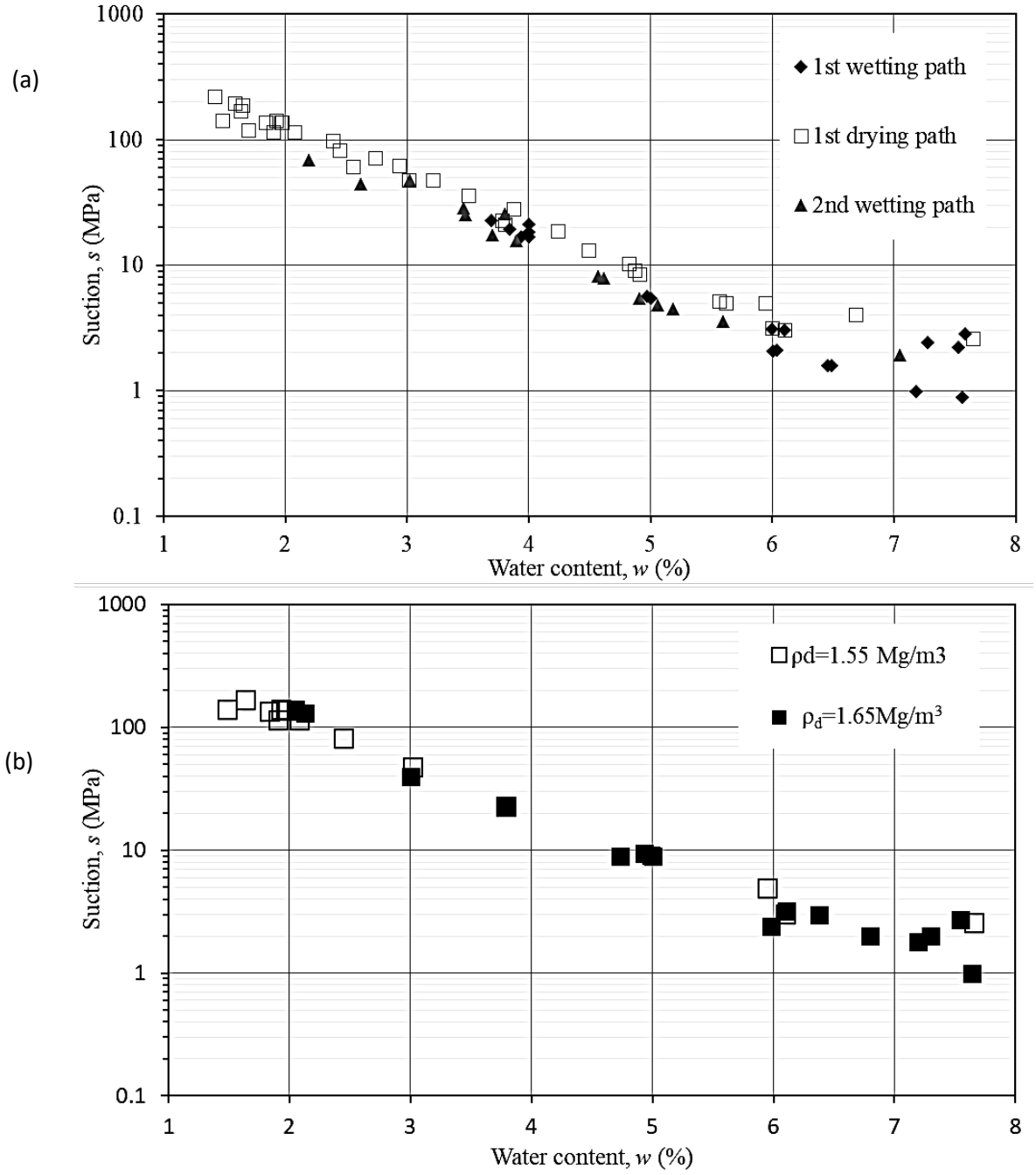

Figure 3. Water retention curves of the sand/silt mixture: a) for drying and wetting paths; b) for two different dry densities.

Three oedometer tests under saturated conditions have been carried out on specimens compacted at different dry densities (1.55Mg/m^3, 1.65Mg/m^3, and 1.75 Mg/m^3) to determine compressibility parameters. A unique one-dimensional normal compression

line (1D-NCL) for the sand/silt mixture cannot be obtained, indicating a 'transitional' mode of compression behavior. However, compressibility parameters are very similar for the three tests (post-yield elastoplastic saturated compressibility index, $\lambda(0) = 0.11$, and elastic compressibility index, $\kappa = 0.01$). In addition, a well-defined increase of the saturated pre-consolidation vertical stress has been detected when the initial dry density increases (σ'_{v0}= 12kPa, 14kPa, and 20kPa, respectively).

Figure 4 presents the oedometer compression curves obtained for three specimens compacted at a water content of 4% and different initial compaction densities.

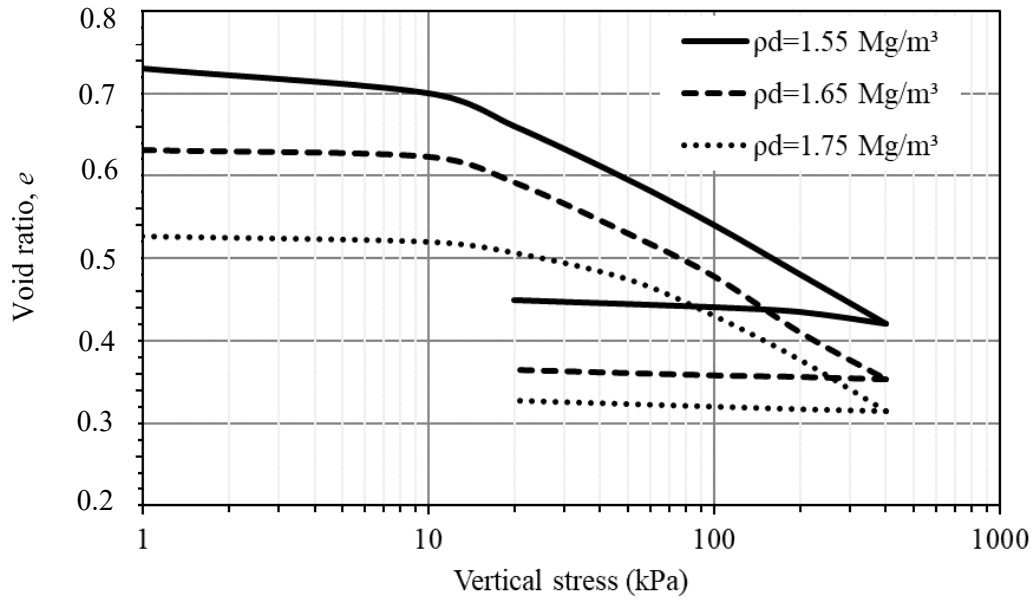

Figure 4. Compression curves obtained in oedometer tests on saturated samples of sand/silt mixture for different dry densities after compaction at w=4.0%.

3 EQUIPMENT AND TEST PROGRAM

Conventional direct shear tests were performed in saturated and at constant as-compacted water content conditions to define the shear strength envelopes on specimens compacted at dry density of 1.65 Mg/m^3 and water content of w=4.0%. Vertical stresses of 50 kPa, 100 kPa, and 200 kPa were applied in the tests. In addition, one test was conducted under saturated conditions with vertical stress of 400 kPa. Undrained triaxial compression tests

were also performed on saturated samples, initially compacted at 4%, 6%, and 8% water contents. Isotropic stresses (p_0') ranging from 200 to 1600 kPa were applied before starting the deviatoric stress stages.

A hollow cylinder apparatus (HCA), as presented in Figure 5, was used (Serra and Hooker, 2003) to perform HM tests under a generalized stress state. The figure also presents the geometrical and stress-strain variables used throughout the paper. This device allows controlling the values of four stress variables (Hight et al., 1983). The variables can be the three principal stresses and the angle between the orientation of the major principal stress and the vertical direction (σ_1, σ_2, σ_3, and α_σ in Figure 5), or the stresses in the vertical, radial, and circumferential directions and shear stress (σ_z, σ_r, σ_θ, and $\tau_{\theta z}$ in Figure 5). The equipment can apply four actions to control the four stress parameters during the tests on the specimen: vertical load (W), torque (T), and internal and external pressures (P_i and P_0, respectively). The orientation of the principal stress has always been vertical, and the shear stress $\tau_{\theta z}$ has been maintained null. From the mentioned actions, three stress invariants may be evaluated: mean stress, (p), deviatoric stress (q), and Lode angle or the parameter b (see Figure 5). The equipment automatically controls the actions to be applied to the specimen to follow any stress path defined in terms of the stress invariants. On the other hand, the response of the soil is characterized through the axial (ΔH), inner (w_i=Δr_i) and outer (w_0=Δr_0) radial displacements and rotation angle (θ, which has been null in the tests performed). These measurements allow us to evaluate the vertical (ε_z), radial (ε_r), and circumferential (ε_θ) strains as well as the volumetric (ε_v), and shear strain (ε_q) invariants (Hight et al. 1983). Figure 5 shows the relationship between soil strains and displacements. In unsaturated specimens, radial displacements can be evaluated by measuring the change in specimen height (ΔH) and the volume changes in the internal and external chambers (ΔV_i and ΔV_0, respectively). These volume changes are

monitored through the data obtained in the pressure/volume controllers used to apply internal and external pressures (Menzies, 1988). In the hypothesis of infinity stiffness of external cell wall, the variation of specimen radii can be evaluated, taking into account that the sum of the volume increments of inner and external chambers and the soil volume should remain constant. Equations to determine the changes in the internal and external radius at any time during the test were presented in Chaudhary et al. (2002). Subsequently, in Minh (2006) the equations were successfully used to assess the variations in radius and compare them with those measured in tests with the sample instrumented with transducers. Equations 1 and 2 present the expressions for the change of internal and external displacement, respectively.

$$w_i = \Delta r_i = \sqrt{\frac{\pi r_i^2 H_o + \Delta V_i}{\pi (H_o + \Delta H)}} - r_i \quad \text{..... (1)}$$

$$w_o = \Delta r_o = \sqrt{\frac{\pi r_o^2 H_o + \Delta V_i + \Delta V_o}{\pi (H_o + \Delta H)}} - r_o \quad \text{..... (2)}$$

The increment of the volume chamber due to the deformation of the Perspex wall associated with increments of external pressure, which affects the external volume changes (ΔV_0), must be taken into account to correct the soil volume changes. Figure 6 shows the relationship between the chamber volume changes and the applied pressure. Due to the large size of the chamber, the volume change measured is not negligible. The first part of the curve is nonlinear due to the presence of air bubbles in the chamber and measuring system. This occluded air volume depends on the sample installation process, and it is not the same in each test. The linear part corresponds to the deformation of the cell wall, and the curve's slope remains approximately the same in the test. The uncertainty of the overall volume of the specimen associated with the volume of air bubbles in the chamber was reduced by measuring at the end of the tests the sample's

volume with the paraffin-coated clod method. The suction at the end of the tests was measured only for some samples to verify the changes between the initial and final states. Figure 7 shows a picture of a paraffin coated sample after the end of the test.

The specimens were statically compacted in laterally confined conditions in a metallic mold, applying vertical displacement on both ends until reaching the specified dry density (1.65 Mg/m^3). The height of the specimens was 100 mm, and the internal and external diameters were 60 mm and 100 mm, respectively.

Different stress paths were considered to obtain the yield points and the shear strength properties. During the tests on unsaturated specimens, the samples' initial water content was maintained (4%, 6%, and 8%), and it was assumed that suction changes were negligible according to the retention curves shown in Figure 3b. In addition, the tests in saturated conditions were performed after saturating the specimens with water flow from the bottom to the top cap in the HCA, under low confining stress (30kPa).

In the shear tests, the first step was to apply isotropic stress (usually 200 kPa). A small increase of deviatoric stress q=20 kPa was applied after this initial to set the parameter b to the desired value (0, 0.5, and 0.8). Afterwards, the deviatoric stress was increased following different values of the stress path slope, $\Delta q/\Delta p$. Small changes in the path slope were observed during the shearing. These changes could be explained by discrepancies between the specimen's volume changes considered by the automatic stress control program (which assumes full saturation of the soil) and the real volume change. These small changes in slope were taken into account in the analyses of the results and did not affect the derived conclusions. A summary of the tests performed indicating the initial conditions of the samples and the stress paths followed is shown in Table 1.

(a) (b) (c)

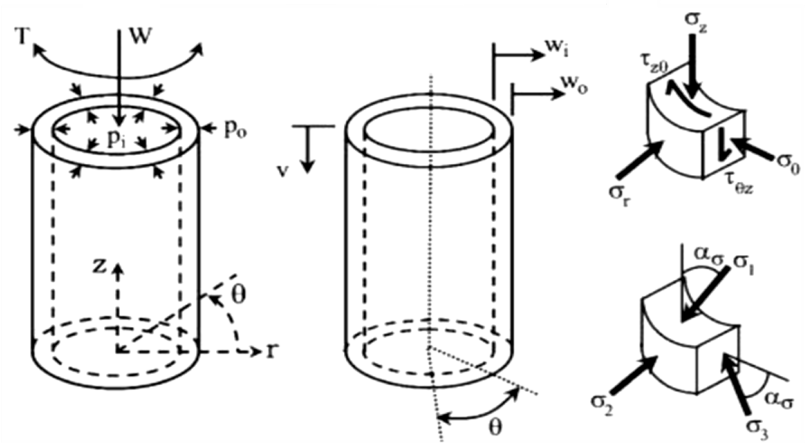

(d)

$$\sigma_z = \frac{W}{\pi(b^2-a^2)} + \frac{(P_o b^2 - P_i a^2)}{(b^2-a^2)} \qquad \sigma_r = \frac{(P_o b + P_i a)}{(b+a)} \qquad \sigma_\theta = \frac{(P_o b - P_i a)}{(b-a)}$$

$$\varepsilon_z = \frac{\delta H}{H} \qquad \varepsilon_r = -\frac{(u_o - u_i)}{(b-a)} \qquad \varepsilon_\theta = -\frac{(u_o + u_i)}{(b+a)}$$

$$\sigma_1 = \frac{\sigma_z+\sigma_\theta}{2} + \sqrt{\left(\frac{\sigma_z-\sigma_\theta}{2}\right)^2 + (\tau_{\theta z}{}^2)} \qquad \varepsilon_1 = \frac{\varepsilon_z+\varepsilon_\theta}{2} + \sqrt{\left(\frac{\varepsilon_z-\varepsilon_\theta}{2}\right)^2 + \frac{\gamma_{\theta z}{}^2}{2}}$$

$$\sigma_2 = \sigma_r \qquad \varepsilon_2 = \varepsilon_r$$

$$\sigma_3 = \frac{\sigma_z+\sigma_\theta}{2} - \sqrt{\left(\frac{\sigma_z-\sigma_\theta}{2}\right)^2 + (\tau_{\theta z}{}^2)} \qquad \varepsilon_3 = \frac{\varepsilon_z+\varepsilon_\theta}{2} - \sqrt{\left(\frac{\varepsilon_z-\varepsilon_\theta}{2}\right)^2 + \frac{\gamma_{\theta z}{}^2}{2}}$$

$$\gamma_{oct} = \frac{2}{3}\sqrt{(\varepsilon_1-\varepsilon_3)^2 + (\varepsilon_1-\varepsilon_2)^2 + (\varepsilon_2-\varepsilon_3)^2}$$

$$\varepsilon_q = \frac{\gamma_{oct}}{\sqrt{2}} \qquad \varepsilon_v = \varepsilon_1 + \varepsilon_2 + \varepsilon_3$$

$$q = \frac{1}{\sqrt{2}}\sqrt{(\sigma_1-\sigma_3)^2 + (\sigma_1-\sigma_2)^2 + (\sigma_2-\sigma_3)^2}$$

$$p = \frac{\sigma_1+\sigma_2+\sigma_3}{3} \qquad b = \frac{\sigma_2-\sigma_3}{\sigma_1-\sigma_3} \qquad \alpha_\sigma = \frac{1}{2}tan^{-1}\left(\frac{2\tau_{\theta z}}{\sigma_z-\sigma_\theta}\right)$$

Figure 5. (a) Sample geometry and applied load/pressures, (b) internal/external radial and axial displacements, (c) stress state in the HCA, and (d) equations for stress and strain variables (adapted from Hight et al., 1983).

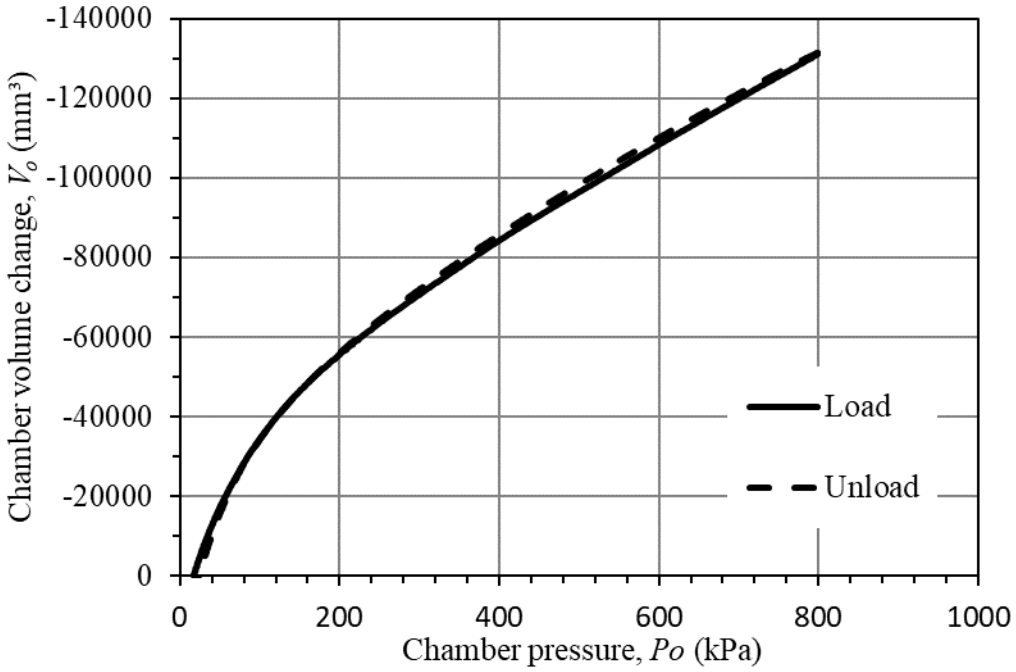

Figure 6. Relationship between the chamber pressure and the volume change of the pressure/volume controller connected to the chamber of the HCA.

Figure 7. Soil sample at the end of the test (left) and after being coated with paraffin (right).

Table 1: Initial water contents and stress paths followed in the tests performed.

$w_{compaction}$ (%)	b	p_o (kPa)	$\Delta q/\Delta p$
4; 6; 8	0; 0.5; 0.8	200	3
4; 6; 8	0	10	0
4; 6; 8	0	200	0.4; 0.75; 0.90; -3
4	0.8; 0.5	200	∞
6	0.2	200	3
6	0.5; 0.8	200	0.75; -3

4 SHEAR STRENGTH PROPERTIES

4.1 Direct shear tests

Figure 8a shows the failure envelopes obtained in the direct shear tests on compacted specimens at 1.65 Mg/m^3 in saturated conditions and with a water content of w=4% (Sr=17%, estimated total suction s= 16 MPa). In both cases, the friction angle is almost the same (ϕ=30^o), whereas the cohesion is null in the saturated test and reaches a value of 31 kPa for the unsaturated specimen.

The cohesion influence on shear strength can be considered by adding the value of $p_s=c(s)/\tan\phi$ to the normal stress value to evaluate the corrected stress that incorporates the suction effects. Using this corrected stress, a unique straight line with a null cohesion and a friction angle ϕ=30^o defines the shear strength envelope for saturated and unsaturated states (see Figure 8b for the $c(s)$ expression and the parameters fitted).

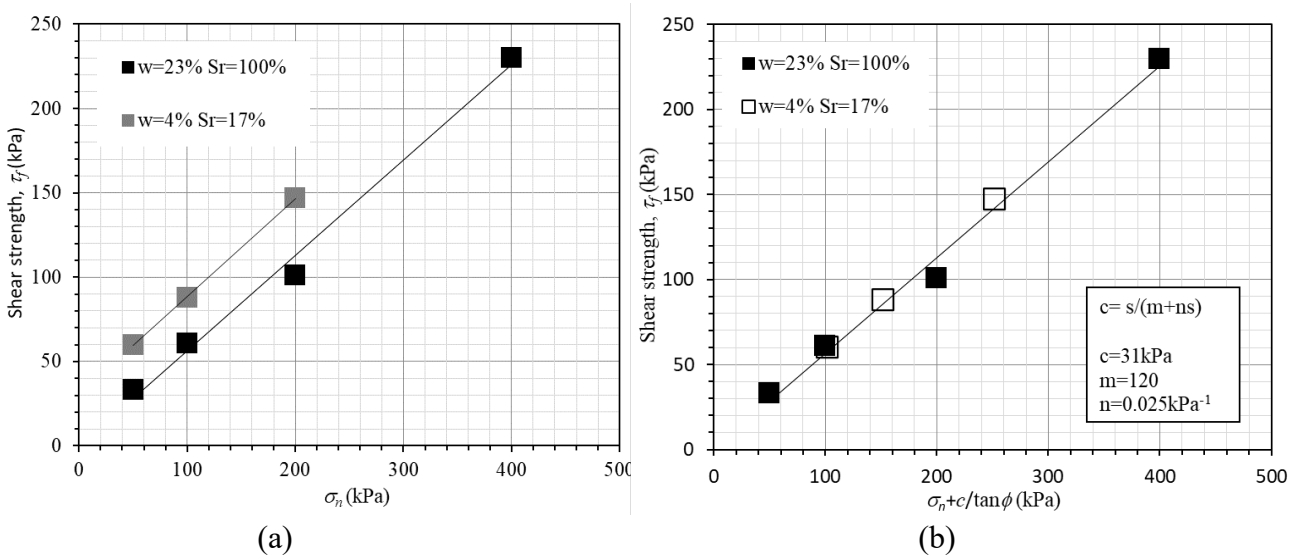

Figure 8. Failure envelopes for the direct shear, without suction correction (a) and with suction correction (b).

4.2 Undrained failure tests in conventional triaxial apparatus

Table 2 shows the failure stresses for samples compacted at different water contents and tested in saturated and undrained conditions following drained compression paths in a triaxial apparatus. A friction angle ϕ=26.5º (M=1.05) was obtained considering the mean value of the results.

Table 2: Failure stresses in undrained triaxial tests on saturated specimen.

$w_{compaction}$ (%)	b	p'_0 (kPa)	q_f (kPa)	p'_f (kPa)
4	0	200	140	130
4	0	1200	1350	1440
6	0	200	160	140
6	0	600	600	610
6	0	1200	1620	1580
8	0	1200	1290	1240

4.3 Generalized stress state tests

Figure 9 shows the influence of parameter b in the stress-strain response in terms of axial strain and deviatoric stress invariant for unsaturated samples tested in the HCA with a water content of 4%, 6%, and 8%. The initial isotropic consolidation stress was 200 kPa, and the shear stress paths were defined by $\Delta q/\Delta p$=3. The effect of the suction in the increment of the shear strength is evident. In addition, it was detected that the sample tested with a parameter b of 0.8 has a lower initial stiffness than the samples tested with values of b of 0 and 0.5. It was also observed that for the same suction, the maximum strength occurred for the tests with parameter b= 0.

On the other side, the volumetric strain responses shown in Figure 10 display different behavioral features. Due to the high value of the initial porosity, the samples experienced a volume reduction. In general, for a value of b=0.5, the volumetric strains are more significant than the strains obtained for the other b values. In addition, for b=0 the volumetric strains have the minimum values. This tendency is more evident in the sample with less water content (w=4%).

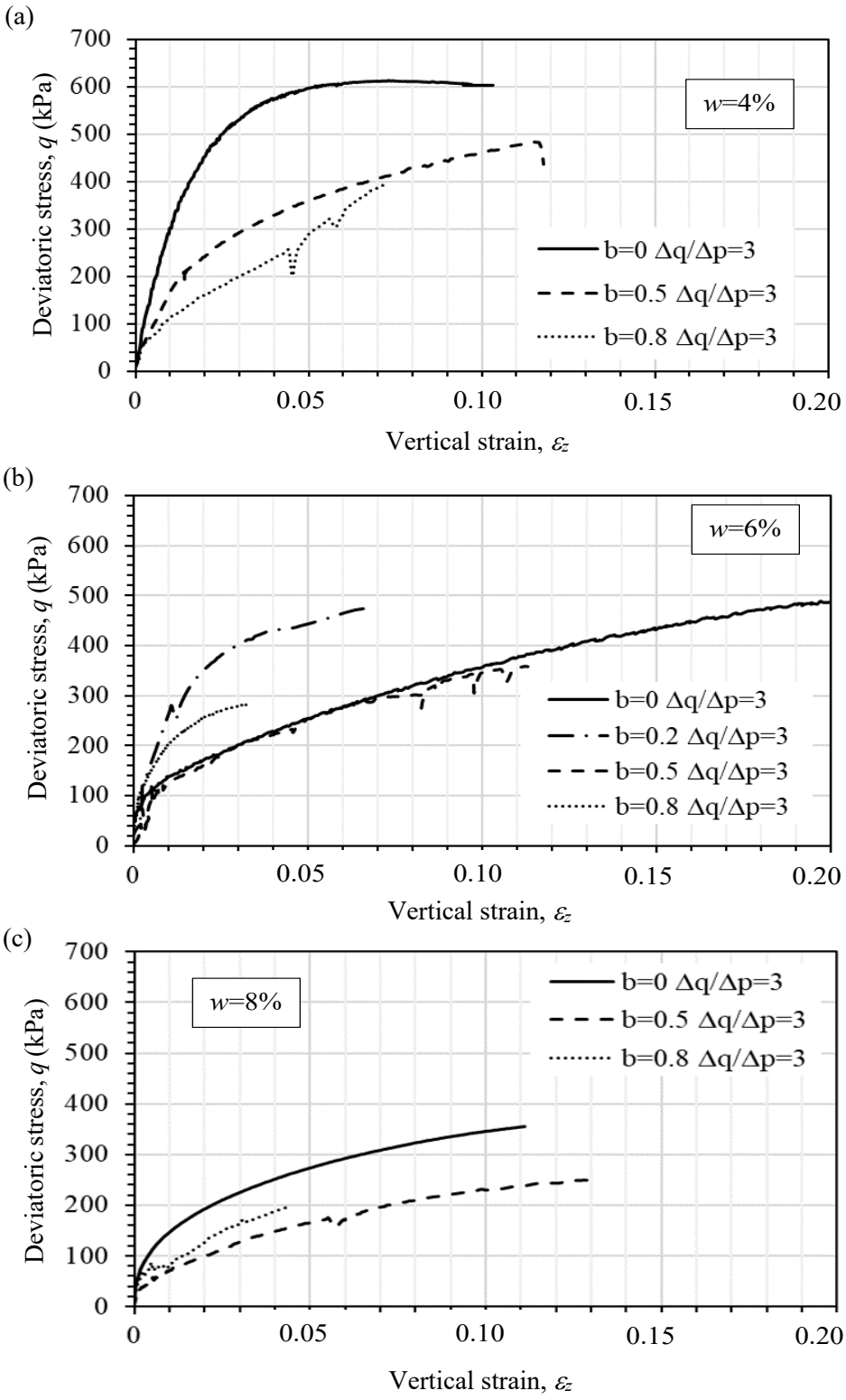

Figure 9. Curves ε_z:q of tests on samples tested in HCA with water content of (a) 4%, (b) 6% and (c) 8%. p_0=200kPa.

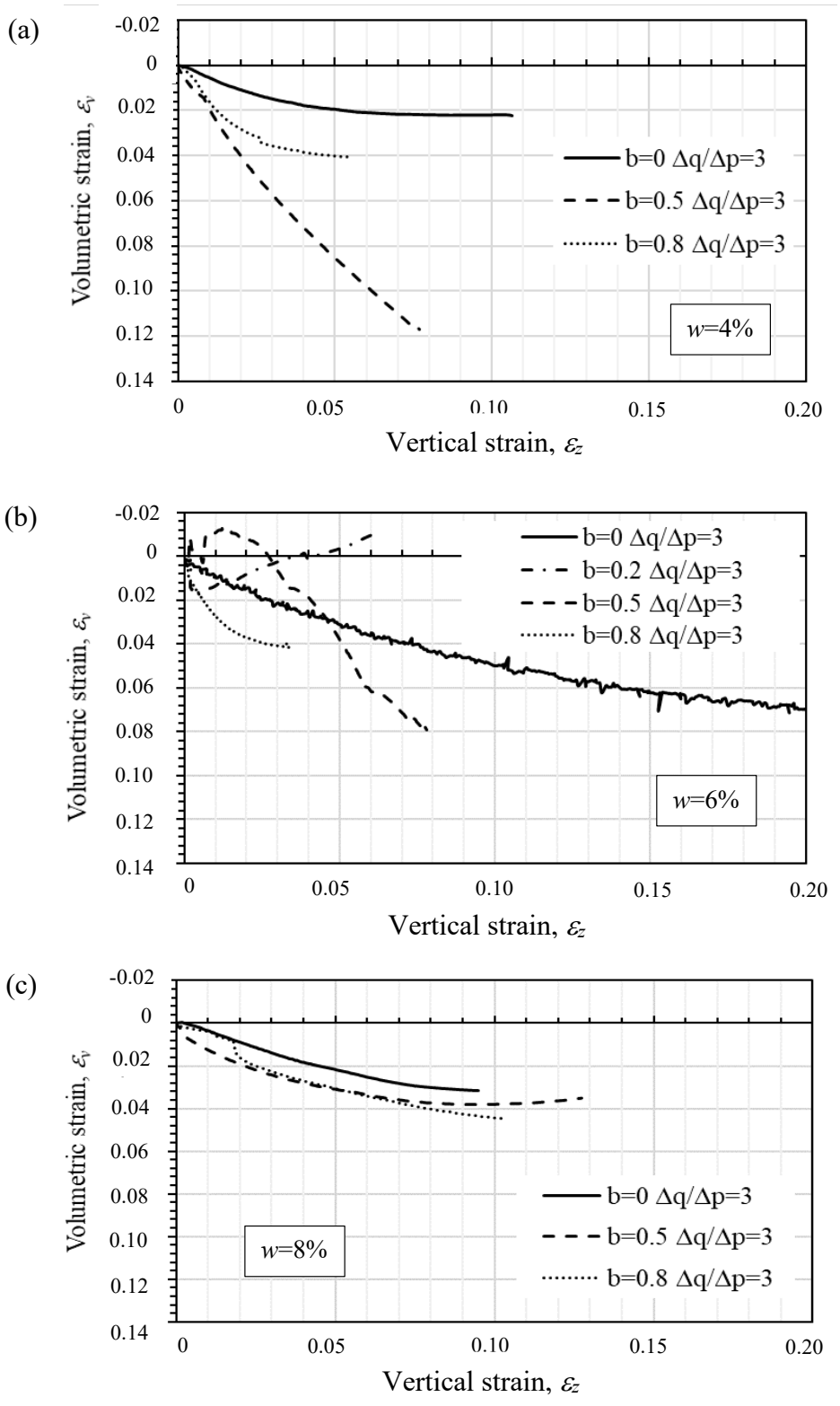

Figure 10. Curves ε_z:ε_v of tests on samples tested in HCA with water content of (a) 4%, (b) 6% and (c) 8%. p_0=200kPa.

In the same way that it has been done with the direct shear tests, the effect of the suction on the strength of the unsaturated soil can be considered by increasing the mean stress value with the term $p_s = c(s) / \tan\phi$. In addition, no effect of suction on the slope $M=q/(p+p_s)$ has been observed. The expression for the strength envelope is presented in Equation 3, where the slope M depends on the parameter b.

$$q = M\left[p + \frac{c(s)}{\tan\phi}\right] \quad (3)$$

The effect of suction changes on the shear strength decreases at high values of suction (Escario and Saez 1986; Escario and Juca,1989; Sun et al.,2000). Consequently, for significant changes of suction, a nonlinear expression of the type $c(s)=s/(m+n\,s)$, where m and n are fitting parameters, can be used for the relationship between cohesion and suction. If $m=1/\tan\phi$ is used, then a hyperbolic expression can be found, where the initial tangent for $s=0$ is $\tan\phi$, which is required by the principle of saturated effective stresses. On the other hand, if $n = 0$, a linear expression is obtained $c(s)=s/m$ with $m=1/\tan\phi_b$, being ϕ_b the angle that defines the effect of suction on the planar envelope of the model presented by Fredlund et al. (1978).

The direct shear and hollow cylinder test results for the shear strength were fitted using equation (3) with the mentioned expression for *c(s),* and the resulting selected parameters were m =120, n = 0.025 kPa^{-1} and ϕ =29°. It should be noted that cohesion c is affected by the suction, but it is not influenced by the Lode angle. The friction angle ϕ is neither affected by the suction nor the Lode angle. Figure 8b shows the shear strength envelope in the case of direct shear tests, and Figure 11 shows the failure envelopes obtained for the tests performed in triaxial and HCA at different water contents (suctions values) and stress conditions according to different values of b. It can be observed that considering

the effect of suction on the strength through the cohesion presents a good performance in fitting the results.

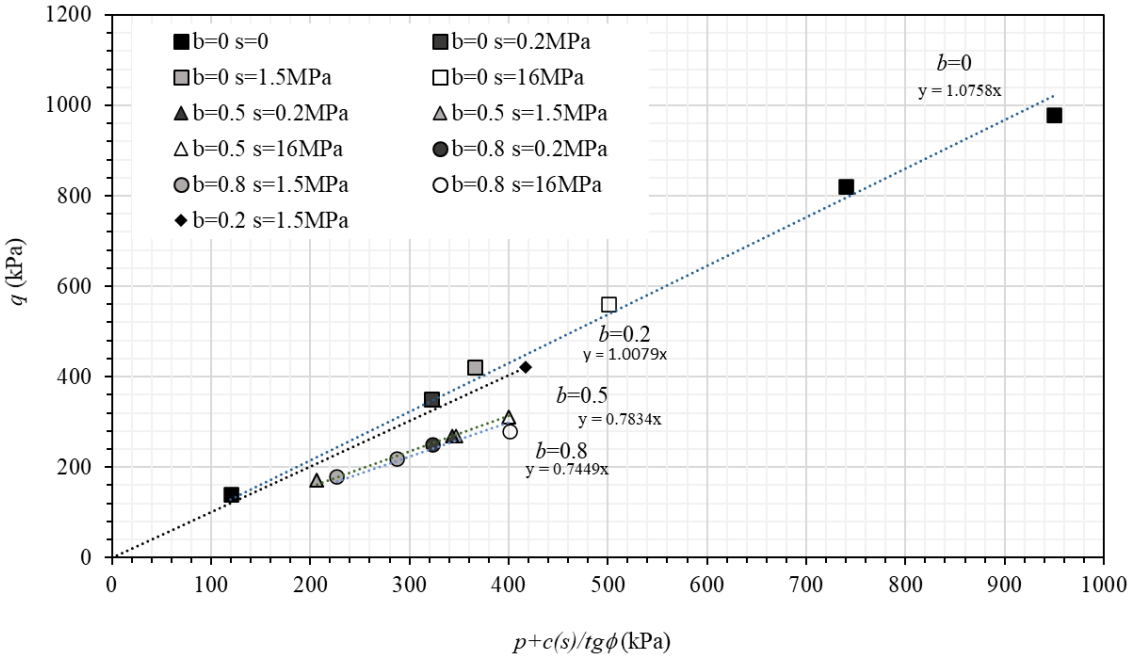

Fig. 11. Shear strength envelopes for different values of the stress parameter *b* and different suctions. The effect of suction is considered through cohesion *c*(*s*).

For each Lode angle (θ_L), the shear strength is characterized by the stress ratio, $q/(p+c(s)/\tan\phi)$ at failure, which is equivalent to the slope of the critical state line $M(\theta_L)$. The variation of $M(\theta_L)$ with Lode angle has been fitted through the proposal of Argyris et al. (1974) shown in Equation 4, in which $M_e=6\sin\phi/(3+\sin\phi)$ in extension (b=1) and $M_c=6\sin\phi/(3-\sin\phi)$ in compression (b=0). The Mohr-Coulomb model (Equation 5) has also been considered for the variation of $M(\theta_L)$ (Maïolino and Luong, 2009).

$$M(\theta_L) = \frac{2\,\mu}{(1+\mu)-(1-\mu)\cos 3(\theta_L+30^0)}\, M_c \quad \text{.....}(\mu=M_e/M_c)\text{.....} \quad (4)$$

$$M(\theta_L) = \frac{\sqrt{3}sin\phi}{cos\theta_L+\frac{1}{\sqrt{3}}sin\theta_L\, sin\phi}\text{.....} \quad (5)$$

Figure 12 shows the results of the stress ratio at failure and its adjustment following the model of Argyris et al. (1974) using ϕ =26.8º (μ = 0.724) and the rest of the parameters

indicated in Table 3. The Argyris et al. (1974) model adjusts the results close to b=0 and b=1, but overestimates the resistance in the vicinity of b equal to 0.5.

The predictions of the Mohr-Coulomb model fit better to experimental data than the obtained with Argyris et al. (1974) model, presenting the best fit when the value $c(s)$ is obtained with ϕ=27.7º, m=47.39 and n=0.0208 kPa^{-1} is used. In addition, it was observed that according to the Mohr-Coulomb model, there is not a considerable variation of the resistance for the values of parameter b greater than 0.5, showing a slight strength increase when b approaches 1. This behavior is not observed in the model presented by Argyris et al. (1974), which expects M to decrease continuously with the increase of b (or the Lode angle). Table 3 presents the fitting parameters obtained for all the models used by minimizing the squared error.

Table 3: Fitting parameters for the different models considered

Model / Parameter	ϕ (º)	m	n (kPa^{-1})	Error $\sqrt{\sum_1^N (M_{model} - M)^2 / N}$
Mohr-Coulomb (eq. 5)	27.7	47.39	0.0208	0.04
Argyris et al. (1974) (eq. 4)	26.8	117.16	0.0183	0.07

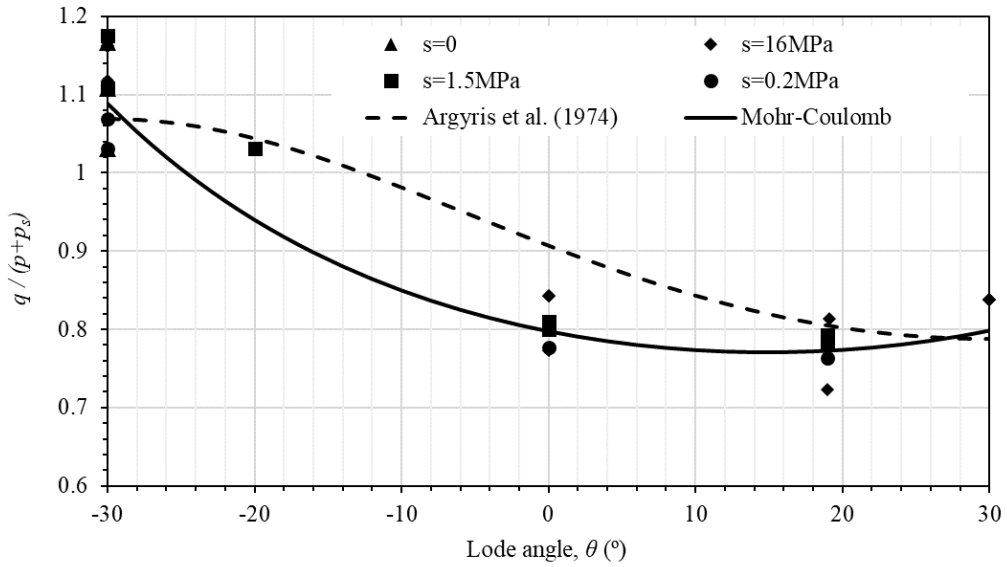

Figure 12. Comparison between Argyris and Mohr-Coulomb models adjusted with the experimental data and parameters shown in Table 3.

5 YIELD SURFACE

5.1 Yield points

The yield points were evaluated by plotting the accumulated plastic work per unit soil volume W_p versus stress vector modulus L (Becker et al., 1987). The plastic work per unit volume was calculated as total work considering elastic strains negligible (Equations 6 and 7), and Figure 13 shows the methodology used to obtain the yield point for a particular case.

$$W_p = \sum(\sigma_1 \delta\varepsilon_1 + \sigma_2 \delta\varepsilon_2 + \sigma_3 \delta\varepsilon_3) \quad (6)$$

$$L = \sqrt{\Delta\sigma_1^2 + \Delta\sigma_2^2 + \Delta\sigma_3^2} \quad (7)$$

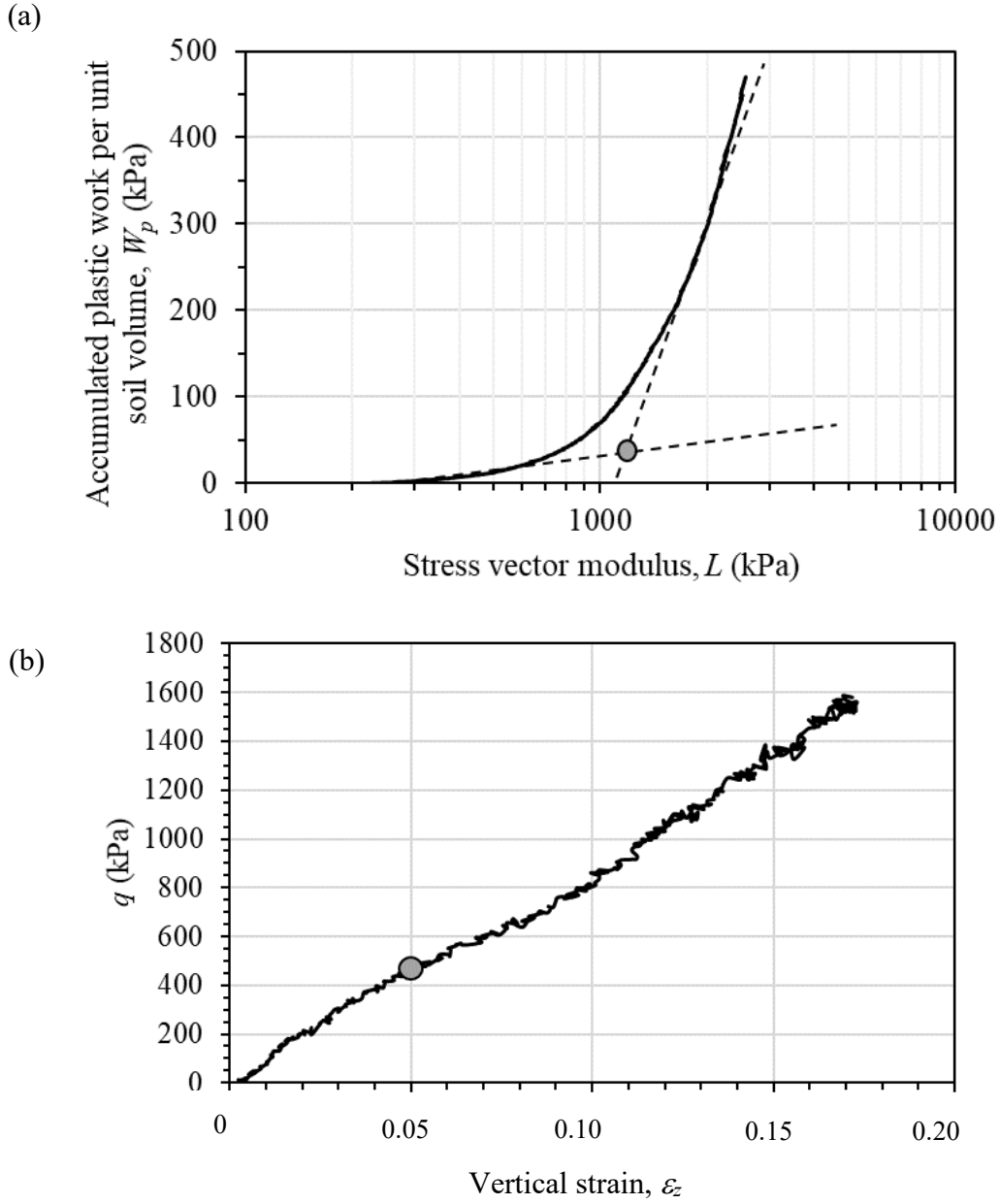

Figure 13. (a) Curve L:Wp and (b) curve ε_z:q in compression test with Δq/Δp=0.75 for a sample compacted at w=4%.

Lagioia et al. (1996) proposed a versatile mathematical expression to describe yield and potential plastic surfaces with a maximum of three parameters. A significant advantage of the model is that it can be adjusted to many surface shapes. The plastic deformations are plotted with a curve in the d-η plane, where $d = \frac{\Delta\varepsilon_v^p}{\Delta\varepsilon_q^p}$ is the dilatancy (changed in sign) and η the stress ratio (q/p). Only two parameters (α and μ) are needed to define this curve, α is the parameter that defines the curvature in the proximity to η=0 where the curve has

a vertical asymptote and μ is associated with the slope of the curve in its final linear section.

Lagioia et al. (1996) model was initially proposed for saturated conditions in conventional compression triaxial tests (b = 0). The original proposal was extended by changing the value of the critical state line slope M to a function $M(\theta_L)$, depending on the angle of Lode. In addition, using the correction to include the effect of suction in unsaturated samples, the stress ratio η in the model of Lagioia et al. (1996) was evaluated as $\eta = q/(p + p_s)$. Equation 8 presents the resulting modified model.

$$d = \frac{\Delta\varepsilon_v^p}{\Delta\varepsilon_q^p} = \mu(M(\theta_L) - \eta)\left(\frac{\alpha M(\theta_L)}{\eta} + 1\right) \quad \text{(8)}$$

The parameters M, μ and α fitted from the experimental tests at different stress states are summarized in Table 4. Figure 14 shows the experimental results at different values of water content and parameter b.

It was observed that the higher the value of b, the lower the proportion η where the curve reaches the critical state with null dilatancy ($\frac{\Delta\varepsilon_v^p}{\Delta\varepsilon_q^p} = 0$). The same behavior occurs for all tests performed with different water content, but the range of variation of the stress ratio in a critical state for the case of b = 0 and the case b = 0.8 varies according to the water content value. A more significant difference in this range of variation was observed for the sample at w=4% (higher level of suction) than for the samples tested at higher w values (Figure 14).

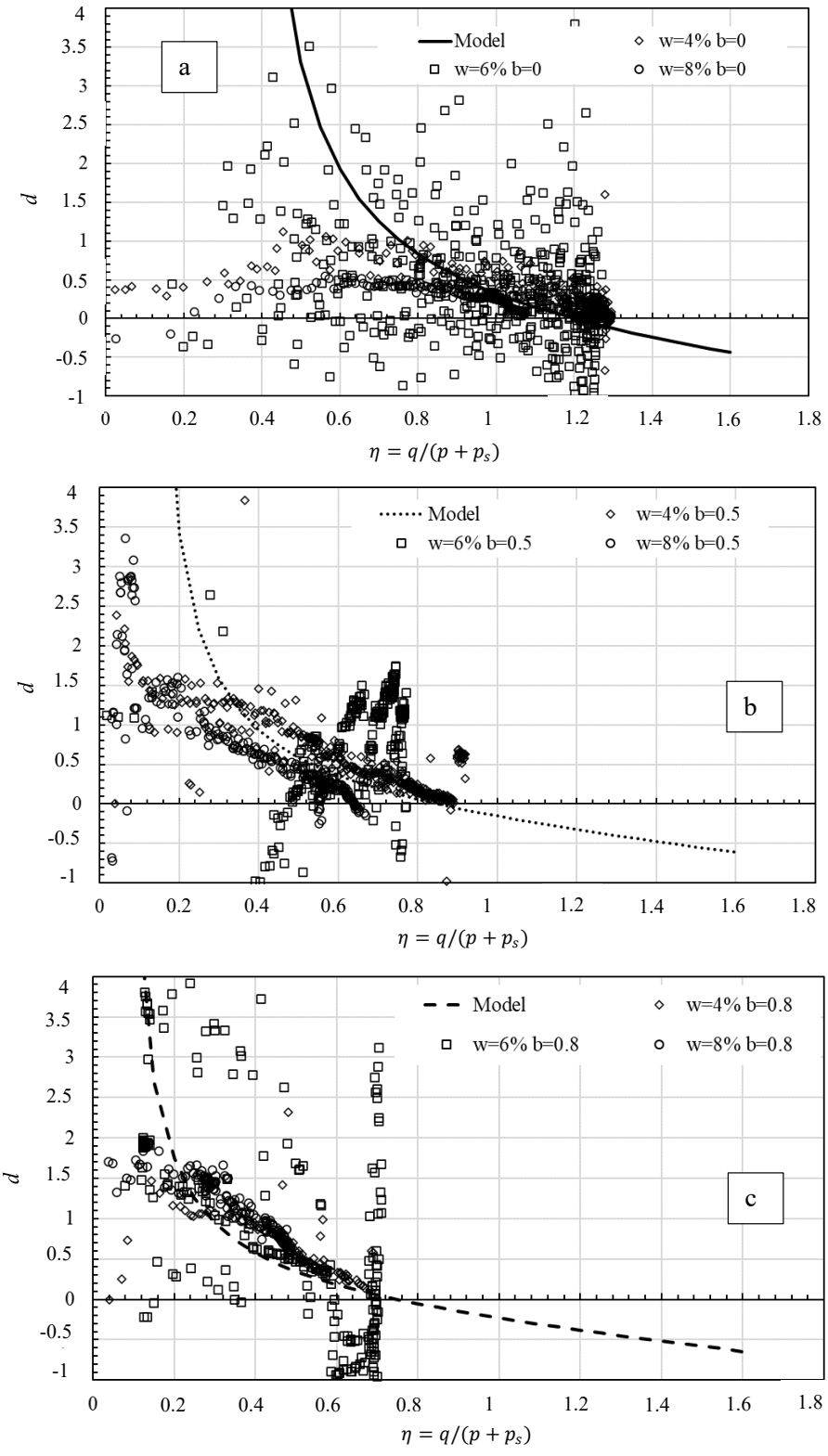

Figure 14. Lagioia et al. (1996) model fitted to the experimental data for soil compacted at different water contents and different values of *b*: *b*=0 (a); *b*=0.5 (b); *b*= 0.8 (c).

Table 4: Parameters fitted for tests on samples with different suctions and using $\eta = q/(p+c(s)/\tan\phi)$ in the modified Lagioia et al. (1996) model (parameters of the cohesion model: n=0.0178 kPa^{-1}, m=43.71; angle of friction: ϕ=27.7º)

b	M	α	μ
0	1.05	0.5	0.99
0.5	0.8	0.5	1.2
0.8	0.75	0.5	1.8

5.2 Isotropic model for b=0

The Barcelona Basic Model (Alonso et al., 1990) can be used to define the shape of the yield surface in the *p*-*q* plane (Equation 9) for the soil after the compaction. The slope of the critical state line (M=1.05) was obtained through the tests in saturated conditions, and p_0 is the parameter that defines the size of the yield surface in the (*p*-*q*) plane at different suctions. The model uses the p_s parameter to model the increase in resistance associated with cohesion due to the suction of the material, and it can be obtained graphically or through expressions that correlate both parameters. In this case, the p_s parameter was calculated using the expression $p_s=c(s)/\tan\phi$.

$$q^2 - M^2(p + p_s)(p_0 - p) = 0 \quad \text{..... (9)}$$

In addition, the usefulness of the model of Lagioia et al. (1996) corrected with suction effects was verified. If the associated plasticity hypothesis is considered, the yield surface shapes can be obtained by integrating the equation defining changes in plastic deformations with the fitted parameters obtained in the plastic flow curves (Equation 8). Equation 10 describes the resulting yield surface (f) and plastic potential (g) for values of $\mu \neq 1$. The suction effect was included through p_s, and consequently $\eta=q/(p+p_s)$ and $\bar{\eta} = \eta/M$. The constants K_1 and K_2 in Equation 10 are calculated using Equation 11.

$$\left.\begin{matrix} f \\ g \end{matrix}\right\} = \frac{p+p_s}{p_0+p_s} - \frac{\left(1+\frac{\bar{\eta}}{K_2}\right)^{\frac{K_2}{(1-\mu)(K_1-K_2)}}}{\left(1+\frac{\bar{\eta}}{K_1}\right)^{\frac{K_1}{(1-\mu)(K_1-K_2)}}} = 0 \quad \text{..... (10)}$$

$$K_{1/2} = \frac{\mu(1-\alpha)}{2(1-\mu)}\left(1 \pm \sqrt{1 - \frac{4\alpha(1-\mu)}{\mu(1-\alpha)^2}}\right) \quad \text{..... (11)}$$

The estimated yield surfaces for both isotropic models and the yield stresses obtained in the tests are presented in Figure 15 for three water contents. The figure below shows clearly the increase of the yield surface with suction. It is possible to observe that the BBM and Lagioia models present very similar shapes and that both surfaces are better fitted on the left side of the critical line than the ones on the right side. From these results, it can be pointed out that the after-compaction yield surface should present a non-isotropic form.

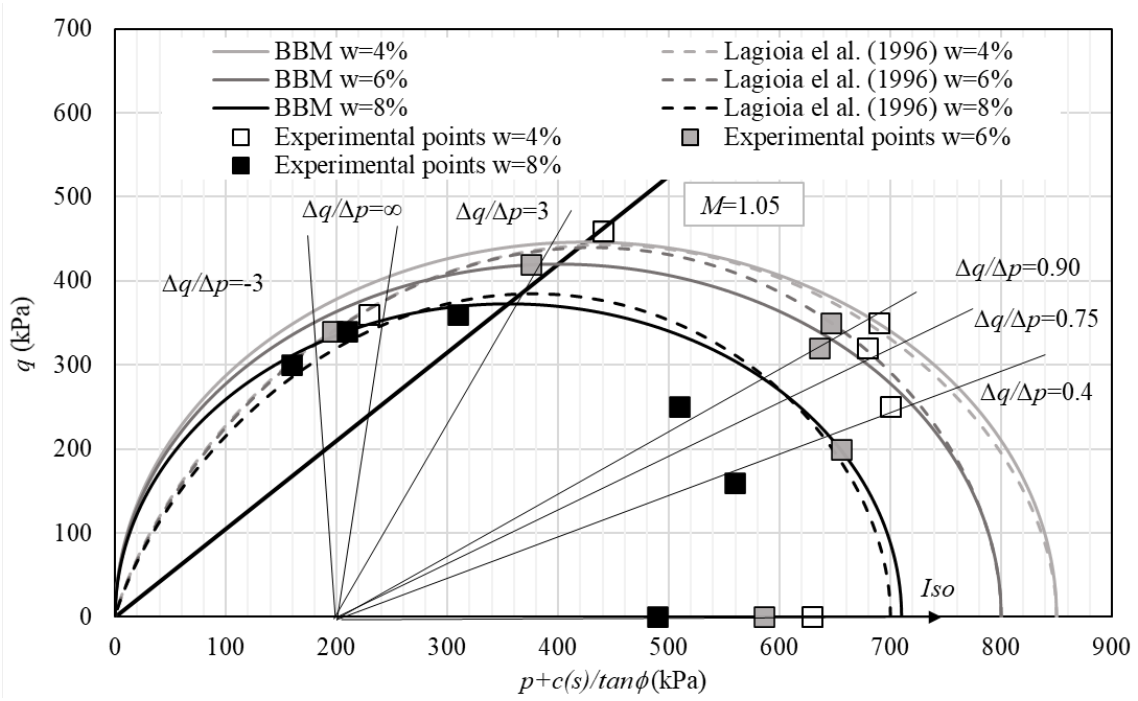

5.3 Anisotropic model for conventional triaxial compression (b=0)

The anisotropic yield surface can be plotted using the model presented by Romero and Jommi (2008), which incorporates the rotation of the yield surface through the inclination M_α. In addition, the parameter p_m defines the size of the inclined yield surface and defines the condition $\partial f/\partial p = 0$, (unlike p_0, p_m does not indicate the crossing point with the axis $q = 0$). The model for the plastic potential and the yield surface is presented in Equation 12, where the effect of suction has been incorporated by adding to the net mean stress (p) the effect of suction through $p_s = c(s)/\tan\phi$, resulting in $\hat{p} = p + p_s$:

$$f = g = (q - M_\alpha \hat{p})^2 - (M^2 - M_\alpha^2)(\hat{p})(p_m - \hat{p}) \quad \text{..... (12)}$$

The parameter p_m can be obtained from yield points experimentally measured through Equation 12. The value of the slope M_α after compaction ($M_{\alpha 0}$), can be obtained from the value of the ratio of the volumetric and shear strains changes in one-dimensional static compaction according to Equation 13:

$$\left.\frac{\dot{\varepsilon}_v}{\dot{\varepsilon}_s}\right\|_{oed} = \frac{3}{2} \cong \frac{d\varepsilon_v^p}{d\varepsilon_s^p} = \frac{M^2 - \eta_0^2}{2(\eta_0 - M_{\alpha 0})} \quad \text{..... (13)}$$

where η_0 is the stress ratio at compaction, $\eta_0 = \frac{q}{(p+p_s)}$, resulting:

$$M_{\alpha 0} = \eta_0 - \frac{M^2 - \eta_0^2}{3} \quad \text{..... (14)}$$

Figure 16 shows the yield points experimentally obtained for suctions of 16MPa, 1.5 MPa, and 0.2 MPa. The adjusted yield surfaces are presented in the same figure. It is possible to observe that the anisotropic model (Romero and Jommi, 2008) fits better than isotropic models to the experimental data, showing the same initial rotation surface due to the compaction for the different suctions. In addition, the consideration of suction

effects with $c(s)$ is good for the points on the left side of the critical state line. Table 5 presents the model parameters used in the surfaces shown in Figure 16.

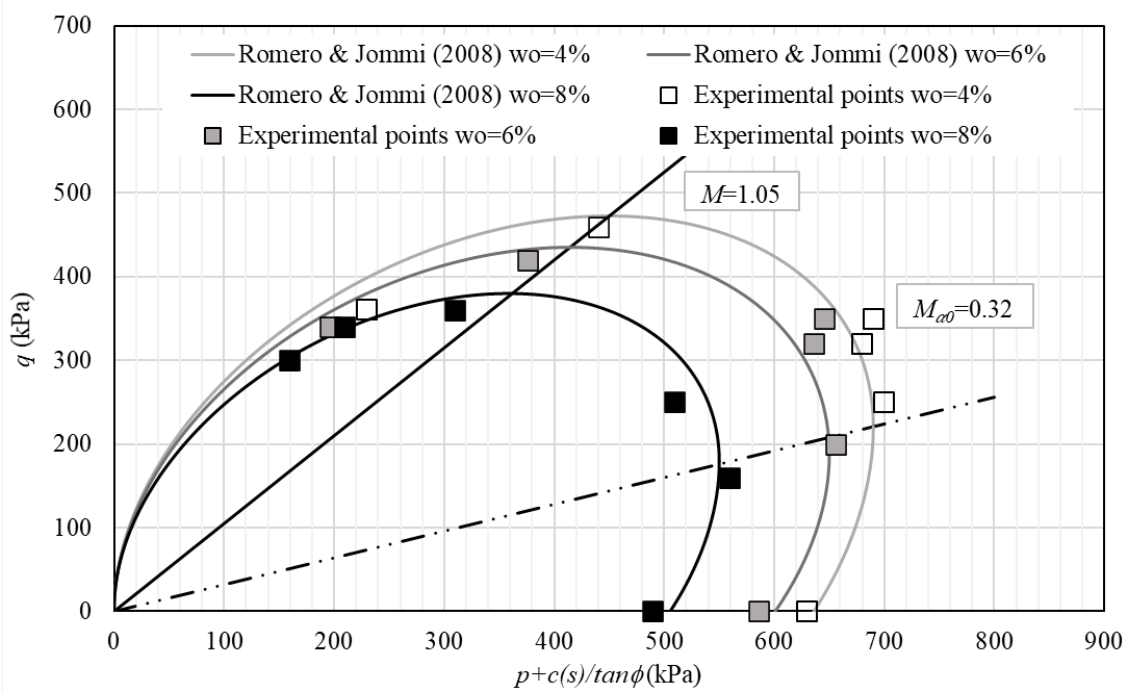

Figure 16. Post compaction anisotropic yield surfaces (Romero and Jommi model) and yield points obtained in tests performed at different water contents and b=0.

Table 5: Parameters for the yield surface models in the cases with b=0 and different suctions, using $p_s=c(s)/\tan\phi$; $c(s)=s/(m+n\,s)$.

				BBM		Lagioia			Romero & Jommi		
s (MPa)	ϕ (°)	m	n (kPa^{-1})	p_0 (kPa)	M	p_0 (kPa)	α	μ	p_m (kPa)	$M_{\alpha 0}$	M
16	27.7	47.39	0.0208	850	1.05	850	0.50	0.99	690	0.32	1.05
1.5	27.7	47.39	0.0208	800	1.05	800	0.50	0.99	650	0.32	1.05
0.2	27.7	47.39	0.0208	710	1.05	700	0.50	0.99	550	0.32	1.05

5.4 Effect of generalized stress state on yield surface using an anisotropic model

The previous sections have established the need to use an anisotropic model to characterize the yield surfaces after compaction in conventional triaxial compression paths (b=0). On the other hand, the effect of suction on these surfaces and the soil strength

can easily be introduced through the apparent cohesion, while the slope of the critical state line and the major axis of the yield surfaces almost do not vary with suction.

The effect of the generalized state of stress (via parameter b) on the slope of the critical state line has also been noted. In this section, the effect of the generalized state of stress on the shape and the size of the yield surfaces will be studied, taking into account the variations of the parameters p_m and M_α in the Romero and Jommi (2008) model.

The Figure 17 presents a scheme of the parameters in the yield surface when parameter b changes. For each Lode angle, θ_L, the critical state has a slope, obtained from the Mohr-Coulomb model, $M(\theta_L)$ in Equation 5. For isotropic compression, the position of the yield point, p_o, is the same for all θ_L. The parameters p_m and $M_{\alpha 0}$ have been fitted from the test results. The graphs in Figures 18, 19, and 20 show the variation of yield surface shape with parameter b and different suctions. Table 6 shows the parameters used for plotting all the cases.

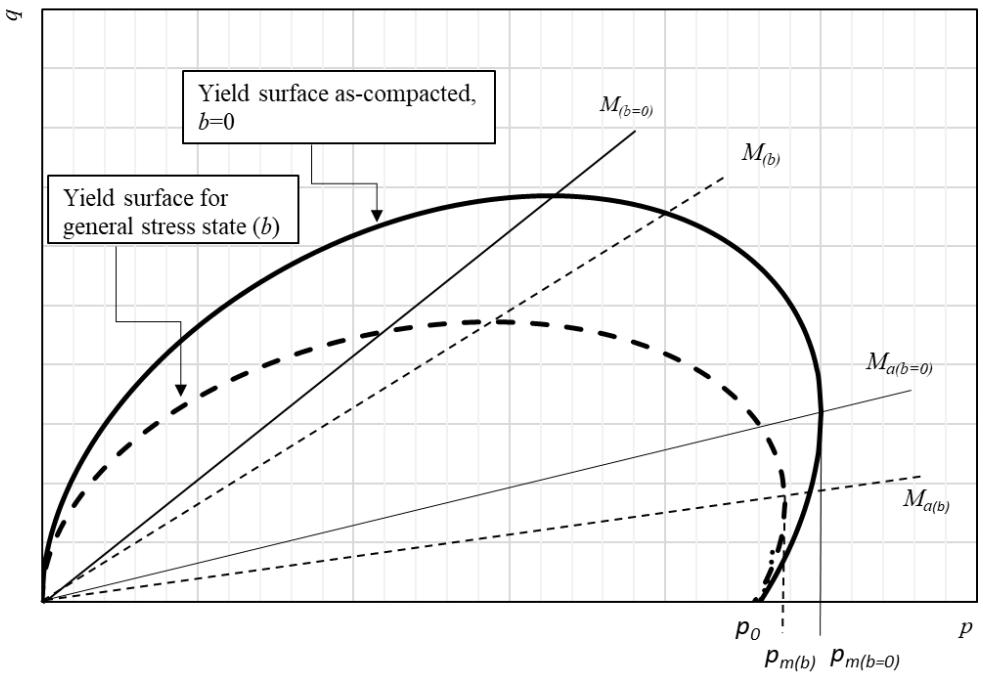

Figure 17. Yield surfaces for different values of the intermediate stress parameter *b* and parameters of the Romero & Jommi model to define the yield surfaces at constant water content.

Table 6. Parameters of Romero and Jommi model at different water contents and stress conditions

w (%)	b	s (MPa)	M	M_α	p_m (kPa)
4	0	16	1.05	0.32	690
4	0.5	16	0.8	0.12	650
4	0.8	16	0.75	0.06	640
6	0	1.5	1.05	0.32	650
6	0.5	1.5	0.8	0.12	600
6	0.8	1.5	0.75	0.06	590
8	0	0.2	1.05	0.32	550
8	0.5	0.2	0.8	0.12	524
8	0.8	0.2	0.75	0.06	514

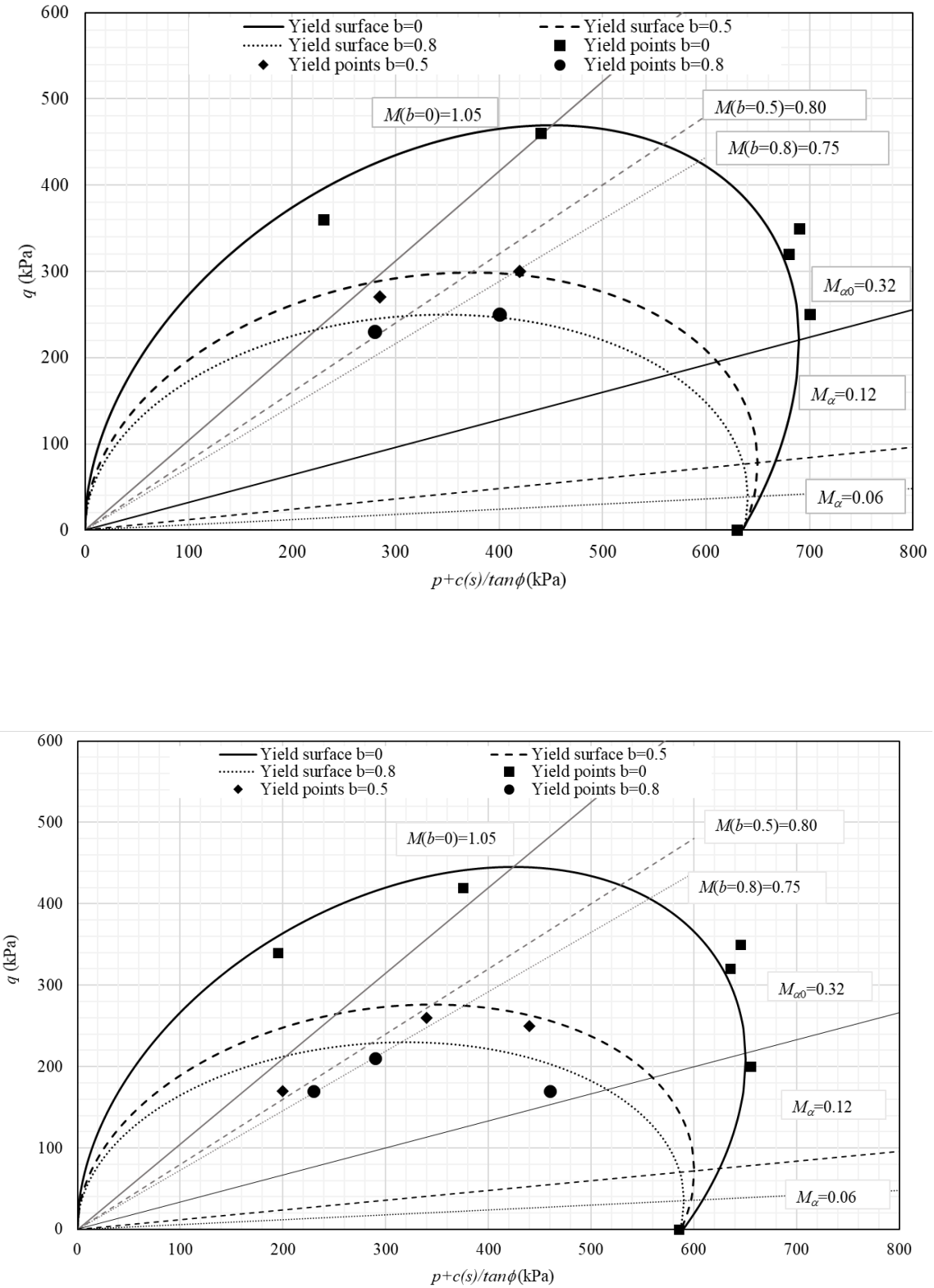

Figure 19: Yield surfaces for different values of *b* for *s*=1.5 MPa using the parameters shown in Table 6.

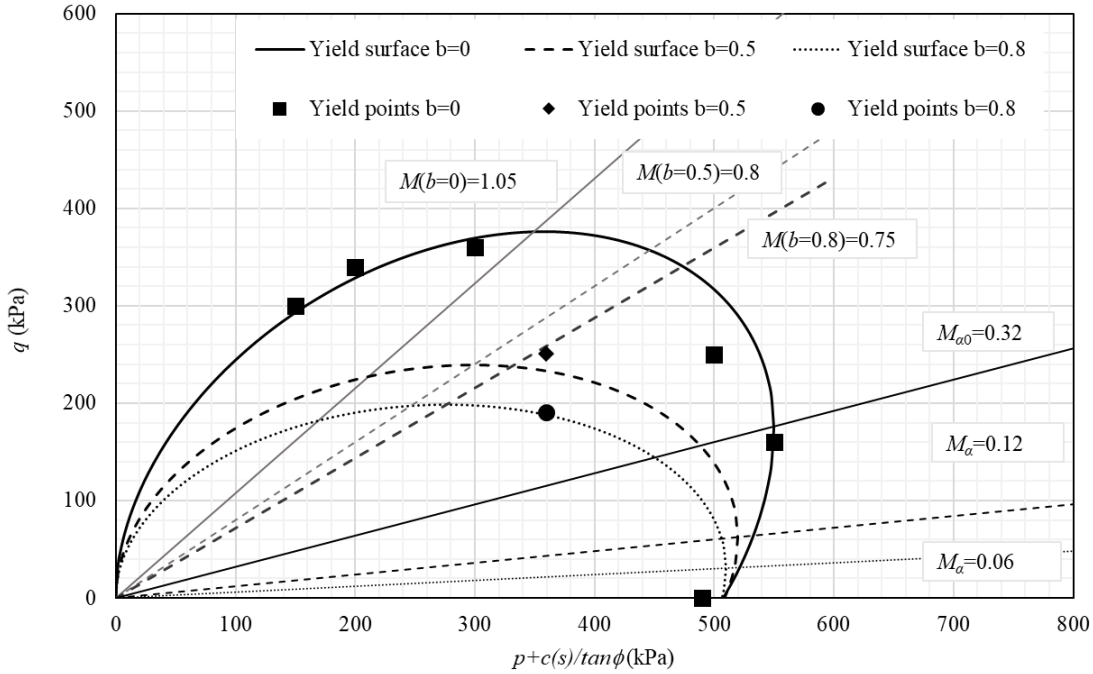

Figure 20: Yield surfaces for different values of *b* for *s*=0.2 MPa using the parameters shown in Table 6.

It was observed that parameter p_m slightly changed due to the intermediate stress parameter (b), whereas the influence of suction on that parameter is more significant. On the other hand, parameter b has a significant influence on the slopes M and M_α, while the suction presents a minor influence on these slopes. M_α decreases from 0.32 to 0.06 when b increases from 0 to 0.8. Figure 21 shows the variation of the parameter p_m as a function b for different suctions. The p_m value tends to decrease slightly (about 8%) for fixed suction values when b varies from 0 to 1. Figure 22 shows the influence of the intermediate stress parameter and the suction on the inclination of the yield surface. To simplify these relationships, one can consider that p_m depends on the suction but not on the stress parameter. On the contrary, M and M_α depend on b, but not on suction.

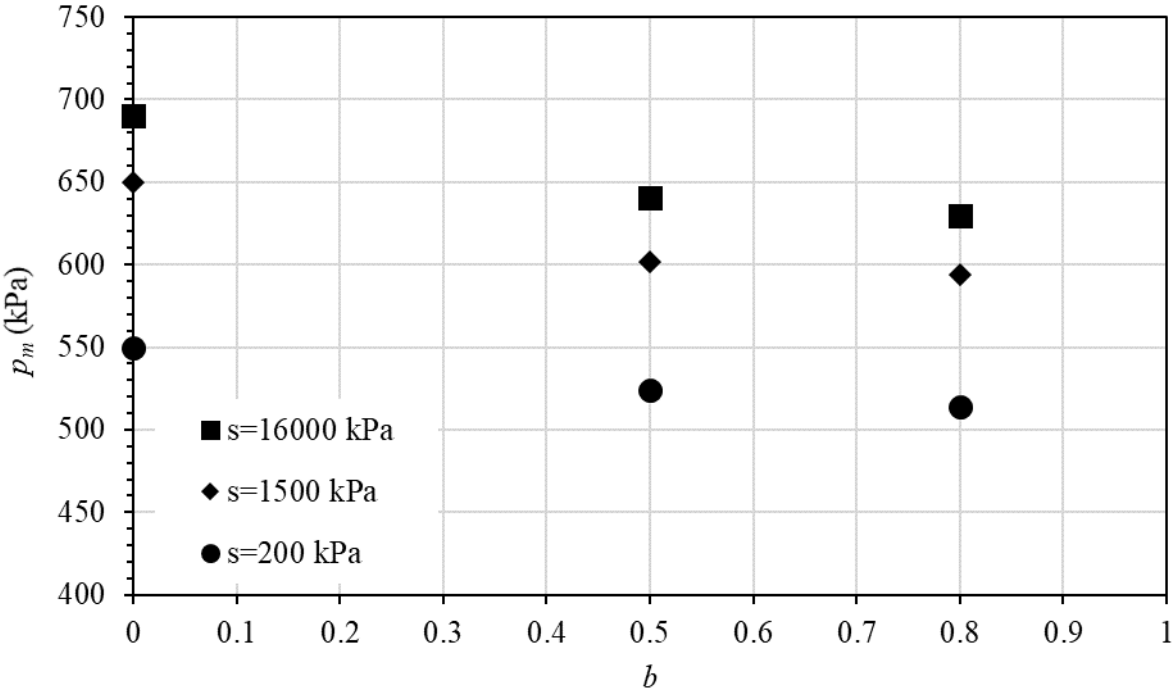

Figure 21. Effects of suction and intermediate stress parameter on the yield surface size parameter, p_m.

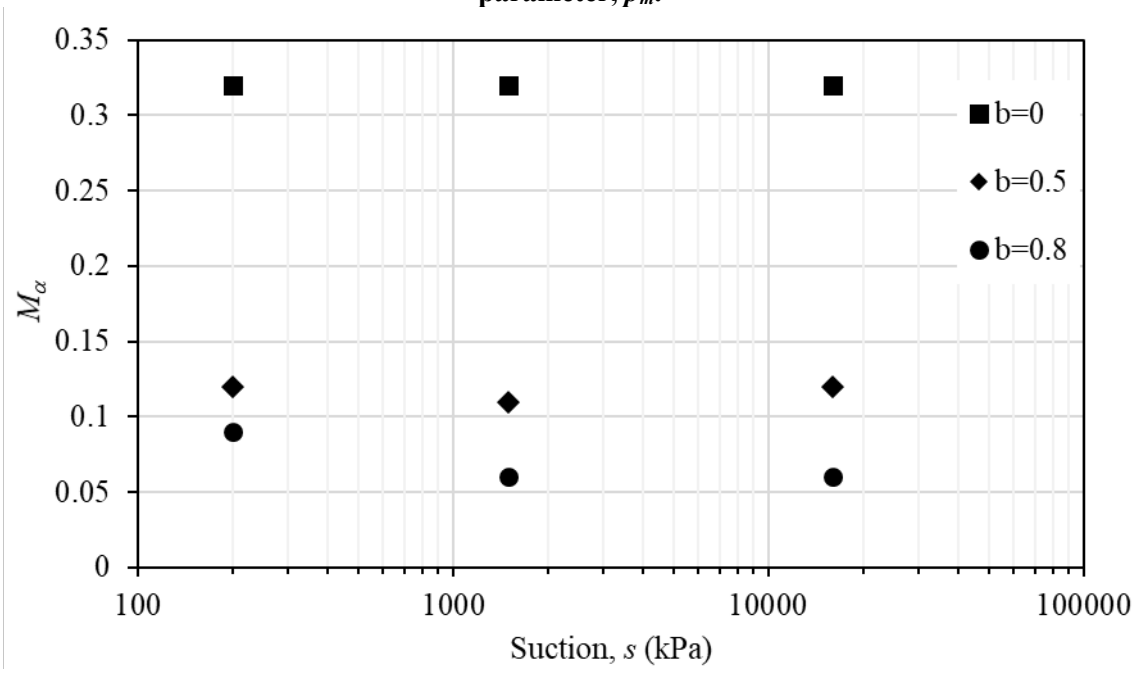

Figure 22. Effects of suction and stress state on the yield surface inclination, M_α.

Disregarding the slight influence of the intermediate stress parameter, the value of the p_m could be approximate using a linear relationship with the logarithm of suction. Equation

15 and Figure 23 present this relationship. For the tests performed, the fitting parameters f_1 and g_1 display values of 31 and 370 kPa, respectively.

$$p_m(s) = f_1\, ln(s+1) + g_1 \quad (16)$$

In the same way, the slope of the yield surface rotation, M_α, can be related to the stress state through the parameter b using the exponential function shown in Equation 17. The fitting parameters are $r = M_\alpha(b=0) = 0.32$ and $t=1.632$. The good fit obtained with this relationship can be observed in Figure 24.

$$M_\alpha(b) = re^{-tb} \quad (17)$$

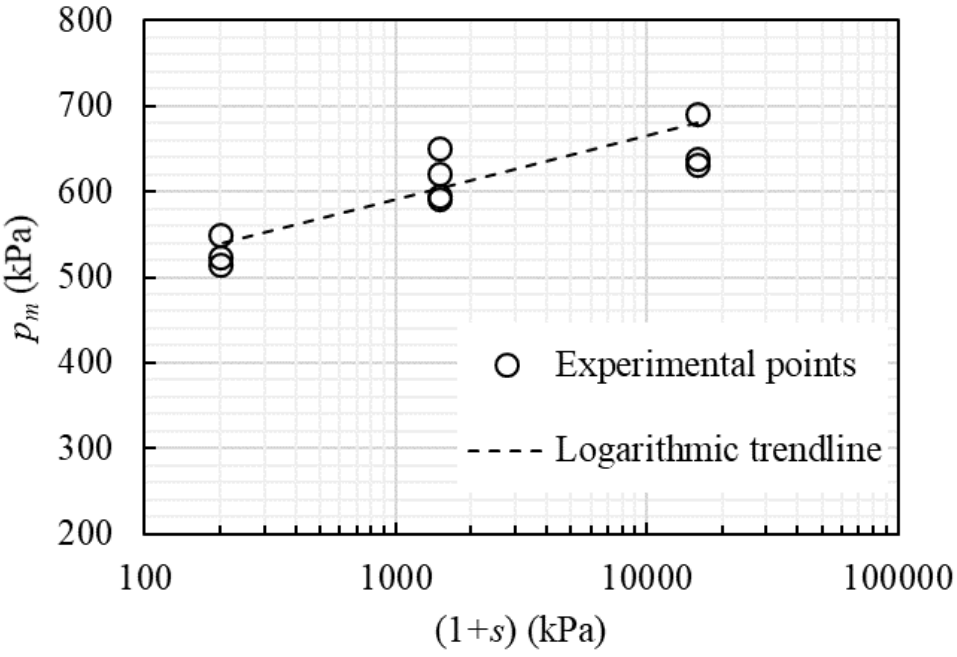

Figure 23. Effect of suction on the parameter p_m of the yield surface for tests performed with different values of b.

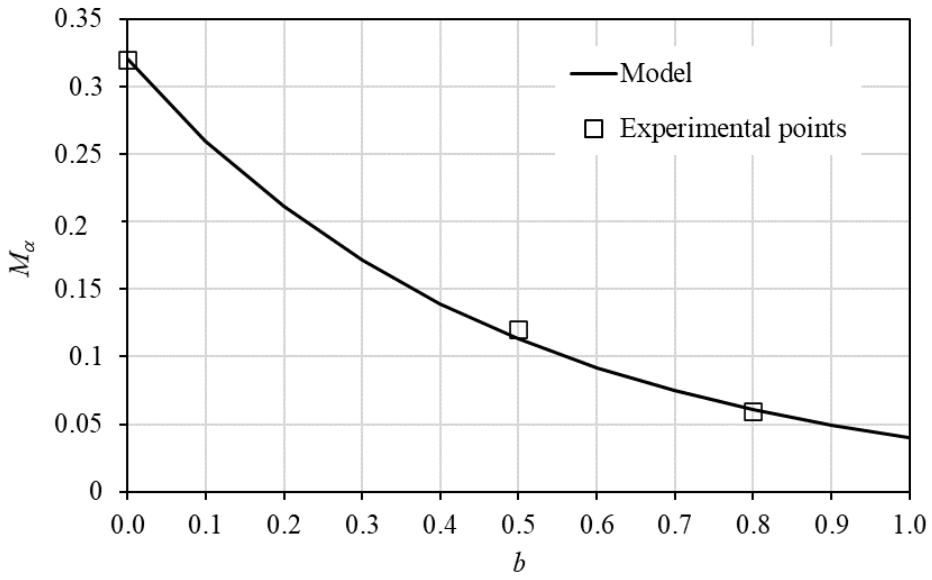

Figure 24. Effect of stress parameter *b* on the inclination of the yield surface for the different tests.

The yield surface of the model of Romero and Jommi (2008) model, Equation (12), can be rewritten using p_0 to normalize the stresses as:

$$f = \left(\frac{q}{p_0} - M_\alpha(b)\frac{p+p_s}{p_0}\right)^2 - \left(M(b)^2 - M_\alpha(b)^2\right)\frac{p+p_s}{p_0}\left(\frac{p_m(s)-p+p_s}{p_0}\right) = 0 \quad \text{..... (18)}$$

Figure 23 shows the relationship between q/p_0 and $(p+p_s)/p_0$ for values of the parameter b=0, 0.5, and 0.8, where p_0 is the isotropic preconsolidation pressure in the unsaturated condition that includes the effect of the apparent cohesion (p_s) (it is the same for all b values at the same water content). The effect of the change of the strength envelope size with b is clearly shown. The values of M and M_α used to draw the normalized yield surfaces are indicated in the same figure. The values of $p_m(s)$ are shown in the fitting curves of Figure 24.

Finally, the yield surface Equation (12) can also be rearranged as:

$$\bar{q} = \frac{M_\alpha(b)}{M(b)}\,\bar{p} \pm \sqrt{\left(\frac{M_\alpha(b)}{M(b)}\,\bar{p}\right)^2 - \bar{p}\left(\bar{p} + \left(\frac{M_\alpha(b)}{M(b)}\right)^2 \overline{p_m} - \overline{p_m}\right)} \quad \text{.....(19)}$$

where:

$$\bar{p} = \frac{\hat{p}}{p_0} = \frac{p + p_s}{p_0} \quad \text{.....(20)}$$

$$\bar{q} = \frac{q}{M(b)p_0} \quad \text{.....(21)}$$

$$\overline{p_m} = \frac{p_m(s)}{p_0} = \frac{1}{1-\left(\frac{M_\alpha}{M}\right)^2} \quad \text{.....(22)}$$

Figure 25 shows the three normalized yield surfaces corresponding to the three different values of the intermediate stress parameter, *b*. The size of the elastic domain increases as the values of *b* decrease, as a consequence of the influence of *b* on *M* and M_α. The relationship between $\bar{p}$ and $\bar{q}$ would be unique if the ratio M_α/M were not dependent on the parameter *b*. Figure 26 shows the ratio between M_α and *M* for the values of *b* and suction used in the tests. From the figure, it can be observed that the ratio M_α/M decreases as the value of the parameter *b* increases. Considering a constant value for the ratio M_α/M = 0.215, and the relationship for $p_m(s)$ and $M_\alpha(b)$ shown in Equations (16) and (17), the Figure 27 shows the resulting normalized yield surface and the points obtained in the testing campaign. Due to restrictions imposed by the assumptions and the dispersion of the experimental results, the discrepancy between the calculated yield surface and measured yield points is appreciable. However, the main phenomena concerning the effects of suction and stress state are included in this simple approach.

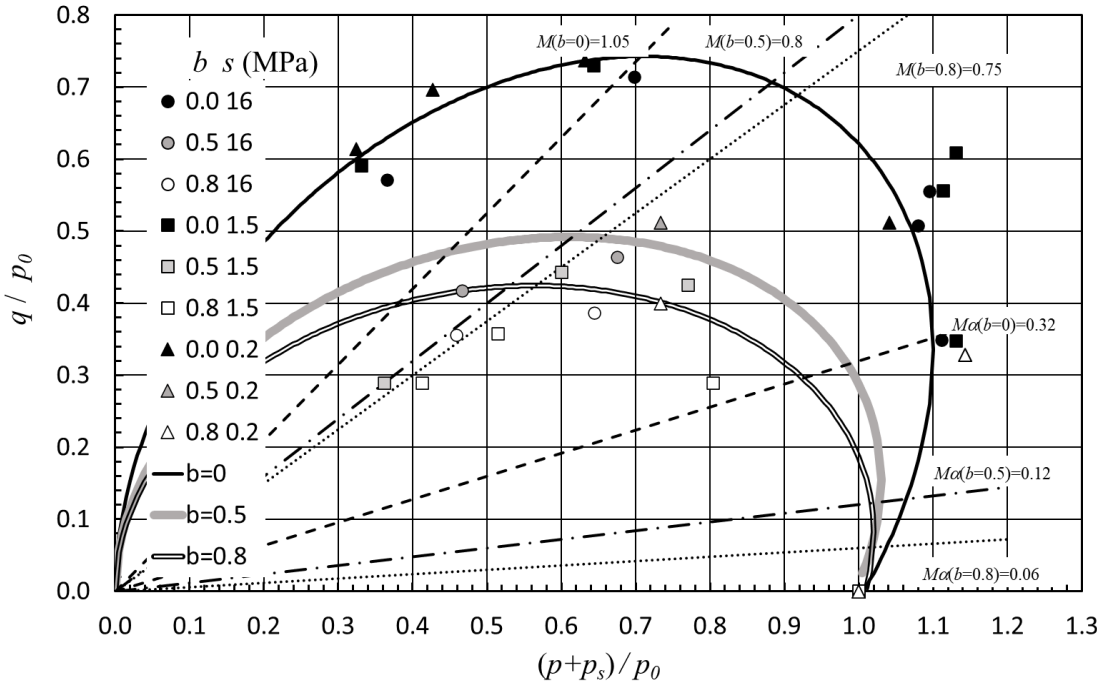
b s (MPa)
0.0 16
0.5 16
0.8 16
0.0 1.5
0.5 1.5
0.8 1.5
0.0 0.2
0.5 0.2
0.8 0.2
b=0
b=0.5
b=0.8
M(b=0)=1.05
M(b=0.5)=0.8
M(b=0.8)=0.75
Mα(b=0)=0.32
Mα(b=0.5)=0.12
Mα(b=0.8)=0.06
q / p0
(p+ps) / p0

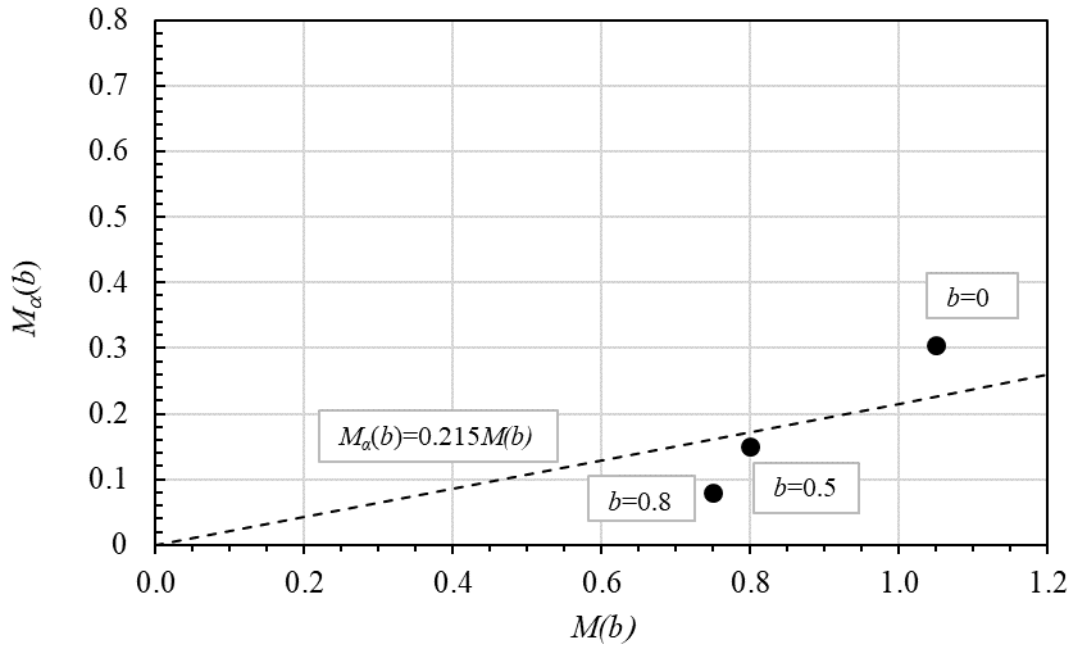
Mα(b)
M(b)
b=0
Mα(b)=0.215M(b)
b=0.8
b=0.5

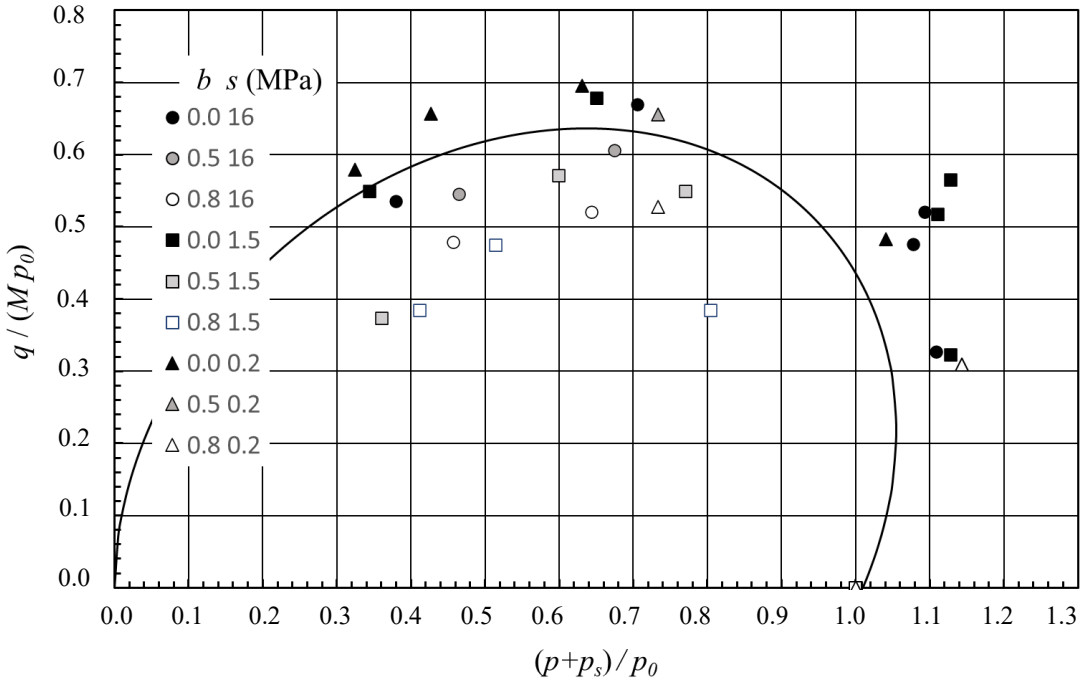

6 CONCLUDING REMARKS

The variation of the shear strength properties and the yield surfaces on a soil compacted at different water contents have been studied, submitted to different generalized stress states. A testing campaign has been performed using a hollow cylinder and conventional triaxial apparatus to evaluate these variations. The effect of suction on strength and yielding can be evaluated considering an equivalent cohesion. It has been established that the strength envelope slope (M) largely depends on the stress distribution through b (or Lode angle) parameter, but the effect of suction on M may be considered negligible. In the tests performed, the effect of b on the slope M can be considered using the Mohr-Coulomb model.

The anisotropic constitutive model proposed by Romero and Jommi (2008) has been successfully adopted to represent the yield surface induced by oedometer compaction. It has been observed that the inclination of yield surface, M_α, mainly depends on stress

parameter b. In contrast, the surface size measured through the parameter p_m depends largely on suction and less on stress state distribution.

It is important to highlight that the suction acts isotropically, increasing the hydrostatic stress, and the stress state parameter should not be influenced. On the other hand, stress state distribution is associated with the deviatoric behavior and influences the shear strength envelope and the yield surface slopes (M and M_α). The parameter p_m indicates the maximum size of the yield surface in the direction of the axis p at given deviatoric stress and depends on its inclination and the applied stress state. Due to the orthogonality between the deviatoric stress variable and the hydrostatic stress variable, the influences from suction and Lode's angle cannot be integrated as a unit.

Empirical relationships between the inclination of yield surface induced during the compaction and the parameter b and between the parameter p_m and suction have been proposed. These relationships allow obtaining the shape of yield surfaces, which can be normalized using different approaches. In particular, a unique normalized yield surface may be obtained if a constant ratio M_α/M is considered for different values of b.

This work has been aimed to discussing the behavior of the yield surface at different stress states and highlight some important points. However, more testing is needed for a better correlation of the variables involved.

7 ACKNOWLEDGEMENTS

The authors acknowledge the financial support of Capes Scholarship Proc. Bex13299/13-1 (Brazil).

8 REFERENCES

Alonso, E.E., Gens, A., and Josa, A. (1990). "A constitutive model for partially saturated soils." Géotechnique, 40 (3), 405-430. [doi: 10.1680/geot.1990.40.3.405]

Alonso, E. E., Pinyol, N. M., Gens, A. (2013) “Compacted soil behavior: initial state, structure and constitutive modelling”. Géotechnique 63(6), 463-478. [doi: 10.1680/geot.11.P.134]

Argyris, J.H., Faust, G., Szimmat, J., Warnke, E. P., and Willam K. J. (1974). “Recent developments in the finite element analysis of prestressed concrete reactor vessels.” Nuclear Engineering and Design, 28(1), 42-75. [doi:10.1016/0029-5493(74)90088-0]

Al-Sharrad, M. A., and Gallipoli, D. (2016). “Incorporating anisotropy in the Barcelona basic model”. In P. Delage, Y.-J. Cui, S. Ghabezloo, J.-M. Pereira, and A.-M. Tang (Eds.), E-Unsat 2016.-E3S Web of Conferences (Vol. 9, p. 17003). [doi:10.1051/e3sconf/20160917003]

Al-Sharrad, M. A., Gallipoli, D. and Wheeler, S.J. (2017). “Experimental investigation of evolving anisotropy in unsaturated soils”. Géotechnique 67 (12), 1033–1049 [doi: 10.1680/jgeot.15.P.279]

Barrera, M. (2002). Estudio experimental del comportamiento hidromecánico de suelos colapsables. PhD thesis, Universitat Politècnica de Catalunya, Barcelona, Spain (in Spanish)

Becker, D. E., Crooks, J. H. A., Been, K. and Jefferies, M. G. (1987). “Work as a criterion for determining in situ and yield stresses in clays”. Canadian Geotechnical Journal, 24(4): 549-564. [doi: 10.1139/t87-070]

Cárdenas, O. E., Weber, R.C., Romero, E., Lloret, A., and Suriol, J. (2015). “Studying collapse behaviour of sandy silt under generalised stress conditions.” Proc. 6th Int. Symposium on Deformation Characteristics of Geomaterials, IOS Press Amsterdam, 462-469, [doi: 10.3233/978-1-61499-601-9-462]

Chaudhary, S. K., Kuwano, J., Hashimoto, S., Hayano, Y. and Nakamura, Y. (2002). “Effects of Initial Fabric and Shearing Direction on Cyclic Deformation Characteristics of Sand”. Soils and Foundations Vol. 42, No. 1, pp. 147-157.

Cui, Y. J. and Delage, P. (1996). “Yielding and plastic behaviour of an unsaturated compacted silt”. Géotechnique, 46(2), 291–311. [doi:10.1680/geot.1996.46.2.291]

Della Vecchia, G. Della, Jommi, C. and Romero, E. (2013). “A fully coupled elastic-plastic hydromechanical model for compacted soils accounting for clay activity”. International Journal for Numerical and Analytical Methods in Geomechanics, 37(5), 503–535. [doi:10.1002/nag.1116]

Escario, V., and Saez, J. (1986). “The shear strength of partly saturated soils”. Géotechnique, 36(3), 453-456. [doi: 10.1680/geot.1986.36.3.453]

Escario, V., and Juca, J. 1989. “Strength and deformation of partly saturated soils”. Proceedings of the 12th International Conference on Soil Mechanics and Foundation Engineering, Rio de Janeiro, Vol. 3, 43-46.

Fredlund, D. G., Morgenstern, N. R., and Widger, R. A. (1978). “The shear strength of unsaturated soils”. Canadian Geotechnical Journal, 15(3), 313-321. [doi: 10.1139/t78-029]

Fredlund, D. G., Rahardjo, H., and Gan, J. K.-M. (1987). Non-linearity of strength envelope for unsaturated soils. Sixth International Conference on Expansive Soils, 49–54. New Dlehi. [doi:10.1016/0148-9062(89)90592-5]

Georgiadis, K., Potts, D. M. and Zdravkovic, L. (2005). “Three-Dimensional Constitutive Model for Partially and Fully Saturated Soils”. International Journal of Geomechanics, 5(3), 244–255. [doi:10.1061/(asce)1532-3641(2005)5:3(244)]

Grammatikopoulou, A., Zdravkovic, L.and Potts,D. M. (2007). “The effect of the yield and plastic potential deviatoric surfaces on the failure height of an embankment”. Géotechnique 57, (10), 795–806. [doi: 10.1680/geot.2007.57.10.795]

Hight, D.W., Gens, A., and Symes, M.J. (1983). “The development of a new hollow cylinder apparatus for investigating the effects of principal stress rotation in soils.” Géotechnique, 33(4), 355-383. [doi: 10.1680/geot.1983.33.4.355]

Hoyos, L. R. (1998). Experimental and computational modeling of unsaturated soil behavior under true triaxial stress state. PhD dissertation, Georgia Institute of Technology, Atlanta.

Hoyos, L. R., Pérez-Ruiz, D. D., and Puppala, A. J. (2012,a). “Refined True Triaxial Apparatus for Testing Unsaturated Soils under Suction-Controlled Stress Paths”. International Journal of Geomechanics, 12(3), 281–291. https://doi.org/10.1061/(asce)gm.1943-5622.0000138

Hoyos, L.R., Pérez-Ruiz, D.D., and Puppala, A.J. (2012,b) “Modeling Unsaturated Soil Response under Suction-Controlled True Triaxial Stress Paths”. International Journal of Geomechanics, Vol. 12 (3), 292-308. [doi: 10.1061/(ASCE)GM.1943-5622.0000159]

Hoyos, L. R., Suescún-Florez, E. A., and Puppala, A. J. (2015). “Stiffness of intermediate unsaturated soil from simultaneous suction-controlled resonant column and bender element testing”. Engineering Geology, 188, 10–28. [doi:10.1016/j.enggeo.2015.01.014]

Jafarzadeh, F., Givi, F.A., and Ahmadinezhad, A. (2019). “Evaluation of the effects of principal stress direction on shear modulus of unsaturated sand using hollow cylinder apparatus”. Earthquake Geotechnical Engineering for Protection and Development of Environment and Constructions- Proceedings of the 7th International Conference on Earthquake Geotechnical Engineering, 2019, pp. 3102-3108.

Kohgo, Y., Nakano, M., and Miyazaki, T. (1993). “Verification of the Generalized Elastoplastic Model for Unsaturated Soils”. Soils and Foundations, 33(4), 64–73. [doi:10.3208/sandf1972.33.4_64]

Kohler, R. and Hofstetter, G. (2008). “A cap model for partially saturated soils”. International Journal for Numerical and Analytical Methods in Geomechanics, 32(8), 981–1004. [doi:10.1002/nag.658]

Lade, P. V. (1997). “Modelling the strengths of engineering materials in three dimensions”. Mechanics of Cohesive-Frictional Materials, 2(4), 339–356. [doi.org/10.1002/(SICI)1099-1484(199710)2:4<339::AID-CFM36>3.0.CO;2-R]

Lade, P. V. and Duncan, J. M. (1975). “Elastoplastic stress–strain theory for cohesionless soil”. J. Geotech. Eng. ASCE, 101(10): 1037–1053. [doi:10.1061/AJGEB6.0000204]Lagioia, R., Puzrin, A.M., Potts, D.M. (1996). “A new versatile expression for yield and plastic potential surfaces”. Comput. Geotech., 19, 171-191. [doi: 10.1016/0266-352X(96)00005-5]

Li, J., Yin, Z. Y., Cui, Y. J., Liu, K. and Yin, J. H. (2019). "An elasto-plastic model of unsaturated soil with an explicit degree of saturation-dependent CSL". Engineering Geology, 260(February), [doi.org/10.1016/j.enggeo.2019.105240]

Li, Z., Zhang, C., Zhao, J., and Yan, Q. (2021). "Safety Factor of Unsaturated Soil Slopes considering the Intermediate Principal Stress Effect and Different Profiles of Matric Suction". Mathematical Problems in Engineering, 1–10. [doi:10.1155/2021/6622522]

Lloret-Cabot, M., Sánchez, M. and Wheeler, S. J. (2013). "Formulation of a three-dimensional constitutive model for unsaturated soils incorporating mechanical-water retention couplings". International Journal for Numerical and Analytical Methods in Geomechanics, 37(17), 3008–3035. [doi:10.1002/nag.2176]

Lu, D., Li, X., Du, X. and Liang, J. (2019). "A simple 3D elastoplastic constitutive model for soils based on the characteristic stress". Computers and Geotechnics, 109(December 2018), 229–247. [doi :10.1016/j.compgeo.2019.02.001]

Ma, C., Lu, D., Du, X. and Zhou, A. (2017). "Developing a 3D elastoplastic constitutive model for soils: A new approach based on characteristic stress". Computers and Geotechnics, 86, 129–140. [doi:10.1016/j.compgeo.2017.01.003]

Macari, E. J. and Hoyos, L. R., (2001). "Mechanical Behavior of an Unsaturated Soil Under Multi-Axial Stress States" Geotechnical Testing Journal, GTJODJ, 24, (1). 14–22. [doi: 10.1520/GTJ11278J]

Macari, E. J., Hoyos, L. R., and Arduino, P. (2003). "Constitutive modeling of unsaturated soil behavior under axisymmetric stress states using a stress/suction-controlled cubical test cell". International Journal of Plasticity (19).1481-1515 [doi:10.1016/S0749-6419(02)00018-9]

Maïolino, S. and Luong, M. P. (2009). "Measuring discrepancies between Coulomb and other geotechnical criteria: Drucker-Prager and Matsuoka-Nakai". 7th EUROMECH Solid Mechanics Conference J. Ambrosio et.al. (eds.) Lisbon, Portugal,12pp.

Maleki, M. and Pouyan, H. (2016). "A kinematic hardening based model for unsaturated soils considering different hydraulic conditions". International Journal for Numerical and Analytical Methods in Geomechanics, 40(16), 2271–2290. [doi:10.1002/nag.2539]

Matsuoka, H. and Nakai, T. (1974). "Stress-deformation and strength characteristics of soil under three different principal stresses". Proceedings of the Japan Society of Civil Engineers, 1974(232), 59–70. [doi:10.2208/jscej1969.1974.232_59]

Matsuoka, H., and Sun, D.A. (1995). "Extension of spatially mobilized plane (SMP) to frictional and cohesive materials and its application to cemented sands". Soils and Foundations, 35(4), 63–72. [doi: 10.3208/sandf.35.4_63]

Matsuoka, H., Sun, D., Kogane, A. Fukuzawa, N., and Ichihara, W. (2002). "Stress-strain behavior of unsaturated soil in true triaxial tests". Canadian Geotechnical Journal, 39 (3), 608-619.[doi: 10.1139/t02-031]

Matsuoka, H., Yao, Y.-P. and Sun, D. (1999). "The Cam-Clay Models Revised by the SMP Criterion". Soils and Foundations, 39(1), 81–95. [doi:10.3208/sandf.39.81]

Menzies, B. (1988). "A Computer Controlled Hydraulic Triaxial Testing System" in Advanced Triaxial Testing of Soil and Rock, ed. Donaghe, R., Chaney, R., and

Silver, M. (West Conshohocken, PA: ASTM International),82-94 [doi: 10.1520/STP29070S]

Minaeian, V., Dewhurst, D. N. and Rasouli, V. (2020). “An Investigation on Failure Behaviour of a Porous Sandstone Using Single-Stage and Multi-stage True Triaxial Stress Tests”. Rock Mechanics and Rock Engineering, 53(8), 3543–3562. https://doi.org/10.1007/s00603-020-02134-y

Minh, N.A. (2006). “An investigation of the anisotropic stress-strain-strength characteristics of an Eocene Clay”. PhD. Thesis. Imperial College London. UK.

Nasreddine, K. (2004). Effet de la rotation des contraintes sur le comportement des sols argileux. These de Doctorat de l'Ecole Nationale des Ponts et Chaussées, Spécialité: Géotechnique. (Enpc), Île-de-France, France. (https://pastel.archives-ouvertes.fr/pastel-00000957).

Nishimura, S., Minh, N.A. and Jardine, R.J. (2007). “Shear strength anisotropy of natural London Clay.” Géotechnique, 57(1), 49-62. [10.1680/geot.2007.57.1.49]

Romero, E., Gens, A., Lloret, A. and Barrera, M. (2003). “Deformation behaviour of anisotropic and isotropic compacted soils due to wetting”. In H. Di Benedetto, T. Doanh, H. Geoffroy, and C. Sauzeat (Eds.), Deformation characteristics of geomaterials, IS Lyon 2003 (pp. 743–749). Lyon.

Romero, E. and Jommi, C. (2008). “An insight into the role of hydraulic history on the volume changes of anisotropic clayey soils”. Water Resources Research; 44,W12412,1-16. [doi: 10.1029/2007WR006558]

Romero E, Cárdenas O.E, Lloret A. and Weber R.C. (2017). “Shear strength properties and collapse response of a sandy silt under generalized stress states”. Proc. 2nd Pan American Conference on Unsaturated Soils, Dallas, USA, 1-10. [doi: 10.1061/9780784481684.036]

Romero, E., Sánchez, M., Gai, X., Barrera, M., and Lloret, A. (2019). “Mechanical behavior of an unsaturated clayey silt: an experimental and constitutive modelling study”. Canadian Geotechnical Journal, 56(10), 1461-1474. [doi: 10.1139/cgj-2018-0117]

Sánchez, M., Gens, A., do Nascimento Guimarães, L., and Olivella, S. (2005). “A double structure generalized plasticity model for expansive materials”. International Journal for Numerical and Analytical Methods in Geomechanics, 29(8), 751–787. [doi:10.1002/nag.434]

Serra, J., Hooker, P. (2003). “A new Computer Controlled Hollow Cylinder Torsional Shear Apparatus”. In: 13th European Conference on Soil Mechanics and Geotechnical Engineering. 471-478. Prague.

Sheng, D., Zhou, A., and Fredlund, D. G. (2011). Shear Strength Criteria for Unsaturated Soils. Geotechnical and Geological Engineering, 29(2), 145–159. [doi:10.1007/s10706-009-9276-x]

Sitarenios, P. and Kavvadas, M. (2020). “A plasticity constitutive model for unsaturated, anisotropic, nonexpansive soils”. International Journal for Numerical and Analytical Methods in Geomechanics, 44(4), 435–454. [doi:10.1002/nag.3028]

Sun, D. A., Matsuoka, H., Yao, Y.-P. and Ichihara, W. (2000). “An Elasto-Plastic Model for Unsaturated Soil in Three-Dimensional Stresses”. Soils and Foundations, 40(3), 17–28. [doi:10.3208/sandf.40.3_17]

Sun, D. A., Matsuoka, H., Cui, H. B. and Xu, Y. F. (2003). "Three-dimensional elasto-plastic model for unsaturated compacted soils with different initial densities". International Journal for Numerical and Analytical Methods in Geomechanics, 27(12), 1079–1098. [doi:10.1002/nag.313]

Sun, D. A., Cui, H. B., Matsuoka, H. and Sheng, D. C. (2007a). "A three-dimensional elastoplastic model for unsaturated compacted soils with hydraulic hysteresis". Soils and Foundations, 47(2), 253–264. [doi:10.3208/sandf.47.253]

Sun, D. A., Sheng, D. C., Cui, H. B., and Sloan, S. W. (2007b). "A density-dependent elastoplastic hydromechanical model for unsaturated compacted soils". International Journal for Numerical and Analytical Methods in Geomechanics, 31(11), 1257–1279. https://doi.org/10.1002/nag.579

Toyota, H., Sakai, N., and Nishimura, T. (2001). "Effects of the stress history due to unsaturation and drainage condition on shear properties of unsaturated cohesive soil." Soils and Foundations, 41(1), 13-24. [doi: 10.3208/sandf.41.13]

Toyota, H., Nakamura, K., Sakai, N. and Sramoon, W. (2003). "Mechanical properties of unsaturated cohesive soil in consideration of tensile stress". Soils and foundations, 43(2), 115-122. [doi:10.1016/S0038-0806(20)30806-4]

Toyota, H., Nakamura, K., and Sramoon, W. (2004). "Failure criterion of unsaturated soil considering tensile stress under three-dimensional stress conditions." Soils and Foundations, 44(5), 1-13. [doi: 10.3208/sandf.44.5_1]

Vanapalli, S. K. (2009). Shear strength of unsaturated soils and its applications in geotechnical engineering practice. In Keynote Address. Proc. 4th Asia-Pacific Conf. on Unsaturated Soils. New Castle, Australia 579-598.

Wang, S., Zhong, Z., Fan, Y. and Liu, X. (2019). "Developing a unified nonlinear strength (UNS) criterion for geomaterials". Arabian Journal of Geosciences, 12(6). https://doi.org/10.1007/s12517-019-4379-z

Wheeler, S. J., and Sivakumar, V. (1995). "An elasto-plastic critical state framework for unsaturated soils." Géotechnique, 45(1), 35–53. [doi: 10.1680/geot.1995.45.1.35]

Wojciechowski, M. (2018). "A note on the differences between Drucker-Prager and Mohr-Coulomb shear strength criteria". Studia Geotechnica et Mechanica, 40(3), 163–169. [doi:10.2478/sgem-2018-0016]

Yan, Q., Zhao, J., Zhang, C., and Wang, J. (2020). "Ultimate Bearing Capacity of Strip Foundations in Unsaturated Soils considering the Intermediate Principal Stress Effect". Advances in Civil Engineering, 2020. [doi:10.1155/2020/8854552]

Yao, C. and Yang, X. (2017). "Limit Analysis of Unsaturated Soil Slope Stability Considering Intermediate Principal Stress and Strength Nonlinearity". Geotech Geol Eng 35, 2053–2063. [doi: 10.1007/s10706-017-0226-8]

Yao, Y. P., Hou, W. and Zhou, A. N. (2009). "UH model: Three-dimensional unified hardening model for overconsolidated clays". Geotechnique, 59(5), 451–469. [doi:10.1680/geot.2007.00029]

Yimsiri, S., Ratananikom, W., Fukuda, F., and Likitlersuang, S. (2011). "Influence of stress rotation and intermediate principal stress on undrained response of Bangkok clay". 14th Asian Regional Conference on Soil Mechanics and Geotechnical Engineering, 23–27. Hong Kong.

Yoshimine, M. (2006). “Generalized Coulomb’s Criterion for 3-Dimensional Stress Conditions”. Soils and Foundations, 46(2), 259–266. [doi:10.3208/sandf.46.259]

Yoshimine, M., Ishihara, K. and Vargas, W. (1998). “Effects of principal stress direction and intermediate principal stress on undrained shear behavior of sand”. Soils and Foundations, 38(3), 179–188. [doi:10.3208/sandf.43.2_115]

Zerfa, F.Z., and Loret, B. (2003). “Coupled dynamic elastic-plastic analysis of earth structures.” Soil Dynamics and Earthquake Engineering, 23 (6), 435-454. [doi: 10.1016/S0267-7261(03)00060-5]

Zhang, C., Chen, X. and Fan, W. (2016). “Critical embedment depth of a rigid retaining wall against overturning in unsaturated soils considering intermediate principal stress and strength nonlinearity”. Journal of Central South University, 23(4), 944–954. [doi:10.1007/s11771-016-3142-9]

Zhang, C., Chen, X., Fan, W., and Zhao, J. (2015). A new unified failure criterion for unsaturated soils. Environmental Earth Sciences, 74(4), 3345–3356. https://doi.org/10.1007/s12665-015-4371-1

Zhang, Ch., Zhao, J., Zhang, Q. and Xu, F. (2010). “Unified Solutions for Unsaturated Soil Shear Strength and Active Earth Pressure”. Experimental and Applied Modeling of Unsaturated Soils. GeoShanghai International Conference, GSP 202. 218–224.

Zheng, F., Shao, S., Wang, J., and Shao, S. (2020). “Experimental Study on the Mechanical Behaviour of Natural Loess Based on Suction-Controlled True Triaxial Tests”. KSCE Journal of Civil Engineering, 24 (8), 2304–2321. [doi:10.1007/s12205-020-1386-2]

Zheng, F., Shao, S., Wang, Y. and Shao, S. (2021). “A new suction-controlled true triaxial apparatus for unsaturated soil testing”. Geotechnical Testing Journal, 44(4). [doi:10.1520/GTJ20190015]